Defining latent EBV load in B lymphocytes: application to multiple sclerosis

Jordana Sheahan

October 2017

Institute for Immunology and Infectious Diseases

School of Veterinary Life Sciences

Murdoch University

A thesis presented for the degree of

Bachelor of Biomedical Science with Honours

Declaration

I declare this thesis is my own account of my research and contains as its main content, work which has not been previously submitted for a degree at any tertiary education institution.

Jordana Sheahan

Abstract

Multiple Sclerosis (MS) is a complex autoimmune and neurodegenerative disease affecting more than 1 in 1000 people. The disease is characterized by T and B lymphocytes attacking the central nervous system, leading to demyelination. This can lead to symptoms affecting the motor function and can result in permanent disability. Epstein-Barr virus (EBV) has been implicated in MS with universal presence and elevated EBV antibody titres in MS patients. The role of B lymphocytes has become of major interest with beneficial effects of B lymphocyte-depleting agents and studies demonstrating increased autoreactive memory-B lymphocytes in MS patients. While EBV is known to reside in B lymphocytes, due to the low EBV copy number during latency it is unknown in which B lymphocyte subset EBV is residing in and if the quantity of EBV infected lymphocytes differs between B lymphocyte subsets in MS patients and healthy controls. The use of a specific and sensitive method to quantitate EBV latency in B lymphocyte subsets is yet to be determined and is the focus of this research study. Three independent methods were compared: Quantitative polymerase chain reaction (qPCR), digital droplet polymerase chain reaction (ddPCR) and flow cytometry coupled with fluorescent in situ hybridization (Flow-FISH) targeting EBV Nuclear Antigen-1 (EBNA-1) and EBER (small viral RNAs), respectively. We have successfully quantified EBNA-1 and EBER in healthy control samples with the techniques qPCR and flow-FISH, respectively. However, as a result of the sequence homology between EBNA-1 and genomic DNA, ddPCR was determined to be too non-specific as it did not quantify target EBNA-1. Phenotyping latently EBV infected lymphocytes could be used in the future as a biomarker for MS diagnosis and to target B lymphocyte depletion therapy more specifically to EBV infected or reactive lymphocytes, limiting side effects and improving patient quality of life.

Acknowledgements

I would like to thank my supervisors, Dr. Monika Tschochner and Prof. Alec Redwood for their guidance and support throughout my honours year and for sharing their knowledge with me.

For their invaluable advice and lab support, I would like to thank Anurahdha Soodha, John Blinco, Francois Rwandamuriya, Abha Chopra and Linda Choo.

For providing and donating samples, I would like to thank the Murdoch University Clinic nurses and study participants.

I would also like to thank my fellow students Dorothy Luk, Jennifer Currenti and Michael Menezes for their friendship, moral support and proofreading skills.

Finally, I would like to thank my partner, Vik, for his loving support, patience and care during my research.

Table of Contents

List of figures

List of tables

1 Abbreviations

APC	Antigen Presenting Cell
ß-ME	ß-Mercaptoethanol
cDNA	Complementary Deoxyribonucleic Acid
CIS	Clinically Isolated Syndrome
CNS	Central Nervous System
CSF	Cerebrospinal Fluid
Cq	Cyclical Value
ddPCR	Digital Droplet Polymerase Chain Reaction
DMSO	Dimethyl Sulfoxide
DNA	Deoxyribonucleic Acid
EBER	Epstein-Barr virus-encoded small RNA
EBNA-1	Epstein-Barr virus Nuclear Antigen 1
EBV	Epstein-Barr Virus
EDSS	Extended Disability Status Scale
ELISA	Enzyme-Linked Immunosorbent Assay
FCS	Fetal Calf Serum
Flow-FISH	Fluorescent in situ Hybridization and Flow Cytometry

HIV	Human Immunodeficiency Virus
HLA	Human Leukocyte Antigen
IFN-ß1	Interferon-ß1
IgG	Immunoglobulin
IM	Infectious Mononucleosis
IL-6	Interleukin-6
LCL	Lymphoblastoid Cell Line
LMP1/2	Latent Membrane Protein 1/2
MBP	Myelin Basic Protein
MHC	Major Histocompatibility Complex
MRI	Magnetic Resonance Imaging
MS	Multiple Sclerosis
PBMC	Peripheral Blood Mononuclear Cell
PBS	Phosphate Buffered Solution
PCR	Polymerase Chain Reaction
PNA	Peptide Nucleic Acid
qPCR	Quantitative Polymerase Chain Reaction
qRT-PCR	Quantitative Reverse Transcription Polymerase Chain Reaction

RFU	Relative Fluorescence Unit
RNA	Ribonucleic Acid
T_H1	T helper cell 1
T_H17 cell	T helper cell 17
T_{reg} cell	T regulatory cell

2 Introduction

Multiple Sclerosis (MS) is a complex autoimmune and neurodegenerative disease characterized by T and B lymphocytes attacking the central nervous system, leading to demyelination. This can result in loss of motor control, vision and vertigo and can lead to permanent disability afflicting more than 1 in 1000 people. Epstein-Barr virus (EBV) has been implicated in MS pathogenesis in many investigations including our own research group, demonstrating universal presence of EBV antibodies in MS patients and additionally elevated EBV antibody titres in MS patients compared to controls. While initial research focussed on T lymphocytes, the role of B lymphocytes has become of major interest with the demonstration of beneficial effects of B lymphocyte depleting agents in MS patients.

EBV is a human herpesvirus that is prevalent in up to 90% of the human population. During the post-infectious stage, the virus enters latency and lies dormant within B lymphocytes with intermittent reactivation. Research has revealed increased autoreactive memory B lymphocytes in peripheral blood and cerebrospinal fluid of MS patients (1–3). These autoreactive B lymphocytes can clonally expand within organs, such as the nervous system, and trigger autoimmune reactions by producing antibodies that bind myelin, leading to degradation.

Furthermore, several studies investigating the association between EBV and MS have discovered symptomatic infection with EBV causing infectious mononucleosis and late infection in life are linked to MS development (4,5). Additional evidence for the importance of EBV in MS pathogenesis is the presence of oligoclonal bands, which are high titers of EBV-specific immunoglobulins specifically observed in the cerebrospinal fluid of MS patients and therefore was used as a diagnostic tool for MS (6,7). For both T and B lymphocytes, molecular mimicry results have been described. T lymphocyte

mimicry occurs if the immune system incorrectly cross-recognizes self-antigens in the brain as part of the immune response (8–10), whilst the mechanism for B lymphocyte mimicry includes EBV cross-reactive antibodies against myelin oligodendrocyte protein (11,12).

EBV persists latently in B lymphocytes and memory B lymphocytes have been discussed as the main reservoir for the virus. Whilst it has been shown in a study by Chaganti, et al., that EBV resides in other B lymphocyte subsets in latent healthy controls (13), it is unknown if the quantity of EBV infected lymphocytes differs between subsets in MS patients and healthy controls. Lastly, EBV viral load, and therefore lytic replication, has not been implicated as a direct cause for MS symptoms, and therefore investigation of latent reservoirs would be of immediate research interest. Unfortunately, viral detection in latency is very difficult and there is currently no single known marker available for the identification of EBV in live cells.

We hypothesize sensitive EBV quantification coupled with B lymphocyte subset targeting will allow the determination of significant differences in the viral load ratio between different B lymphocyte subsets. If this ratio is compared between MS and healthy controls, a specific EBV-infected B lymphocyte subset in MS will be known. EBV quantities in subsets might inform as a biomarker for future MS diagnosis. Additionally, identifying and characterising latently EBV infected lymphocytes could be used in the future to target B lymphocyte depletion therapy more specifically for a subset of B lymphocytes only, limiting side effects and improving patient quality of life.

3 Multiple Sclerosis (MS)

3.1 MS disease progression

During the disease progression of MS, the myelin surrounding the nerves in the central nervous system (CNS) is significantly damaged due to autoimmunity. The white matter and the cortical grey matter of the CNS display histological abnormalities, including inflammatory cell infiltration and physical lesions upon autopsy (14,15). When the myelin degenerates, the axons of nerves are exposed and action potentials are interrupted due to exposed ion channels (16–19). These demyelinated or inflamed areas may be visible on magnetic resonance imaging (MRI) scans and are referred to as 'lesions' in this context (19). Of note, a third of patients may only have benign clinically 'silent' lesions with no accompanying symptoms (20). As a result of demyelination, nerve impulses are slowed, and with subsequent axonal loss associated with disease progression, do not reach the synapse, and therefore the target muscle, leading to a loss of muscle control as the nerve cannot sustain a functional motor impulse.

Long-term, muscle atrophy frequently occurs due to the lack of stimulation by action potentials. This absence of action potential makes movement harder for those suffering from the disease (21). Walking aids are often required to assist with movement and patients can be severely disabled and at risk of falling (22). The development of MS is typically a gradual worsening disability over a patient's lifetime. This progression of disability decreases lifespan by an average of seven years according to a 60-year study in Norway, where mortality is three times higher in MS compared to controls (23).

3.2 Clinical patterns of MS

The progression of MS disease can be categorized by clinical patterns. The precursor category of MS is called clinically isolated syndrome (CIS), where a patient exhibits clinical symptoms indicative of MS for the first time, however, this is not a definite

diagnosis as MS does not always develop after this initial episode. As can be seen in Figure 3.1(a), the most common form of MS is the relapsing-remitting form of MS and is present in about 80% of patients. Relapsing-remitting MS is characterized by symptoms leading to a loss of motor function alternating with periods of recovery and no symptoms (24). It is currently unknown exactly why patients may relapse into MS disease. Next to relapsing-remitting, primary progressive and secondary progressive are distinct types of MS with various levels of symptoms and recovery periods, as illustrated in Figure 3.1(b,c). Relapsing-remitting MS may progress into secondary progressive MS, as depicted in Figure 3.1(c) where the attacks are less regular but the disease gradually worsens with no remission (25). In contrast, primary progressive MS (Figure 3.1(b)) is the rarest form and occurs in only about 5% of patients (26). This form is characterized by a lack of early relapses or remissions but instead progressive worsening of disease (25). Clinically, these categories of MS can only be established after about 10 years of monitoring, but categorizing is required to administer the most appropriate treatment (27). Categorizing by clinical patterns also aids in the diagnosis of MS.

a

b

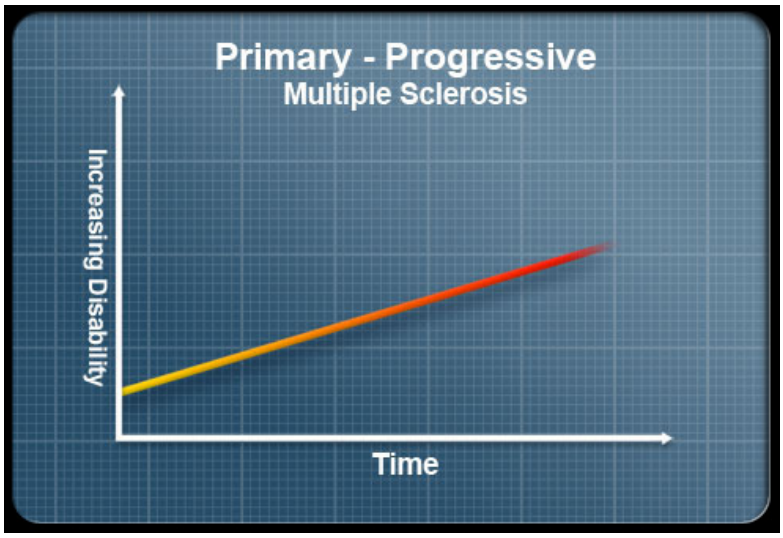

c

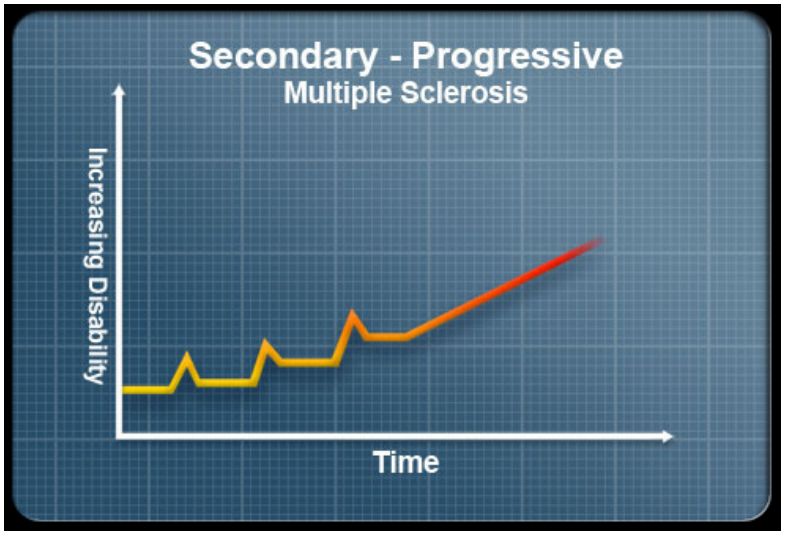

Figure 3.1: Clinical patterns of Multiple Sclerosis (MS): (a) Relapsing-remitting MS involves intermittent relapses and remissions from early on. (b) Primary-progressive is a gradual worsening over time with no remission. (c) Secondary-progressive MS: The disease progressively worsens with no remission (132). *Images from OnHealth 2016 WebMD*

3.3 MS diagnostics

Diagnosis of MS involves a combination of tests, including magnetic resonance imaging (MRI), symptomatic testing and pathology analysis. As portrayed in Figure 3.2, the myelin damage resulting in lesions in the CNS can be directly visualised by MRI, which is the most commonly used tool for MS diagnosis (28). In addition to imaging, functional testing for the determination of disability levels in MS patients is often assessed under the Extended Disability Status Scale (EDSS) (29). The test measures walking ability but it is not designed to measure physical neurological symptoms such as visual problems, cognitive changes, motor control changes in other limbs than the legs, sensory response loss, balance, coordination, and bladder or bowel control (29).

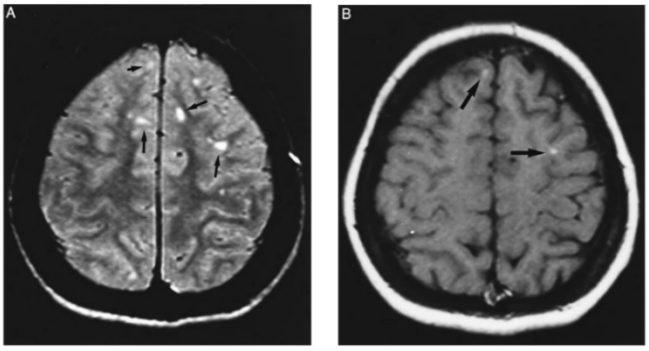

Figure 3.2: Magnetic resonance imaging (MRI) scan of a patient diagnosed with clinically definite multiple sclerosis. Note lesions in the frontal and parietal lobes (A) and lesions within the cortex (B) indicate areas of demyelination. (28). *Images from Barkhof F., et al., 1997, Brain.*

Next to MRI analysis, pathological testing for additional confirmation of MS diagnosis is utilized. The inflammation of the CNS, a hallmark of MS, can be confirmed by harvesting cerebrospinal fluid (CSF) via lumbar puncture. CSF is subsequently assessed for immunoglobulin levels, a sign of the presence of immune cells in the brain (6). Generally, several diagnostic methods are used in conjunction to enable the correct diagnosis and administration of therapy to MS patients.

3.4 MS treatment

There is currently no cure for MS, nor is there a preventative vaccine available. Nonetheless, there are many treatments that can minimise the progression of the disease, but none have been proven to absolutely stop the disease in its tracks, reverse its effects or be effective without side effects. The most current forms of MS treatment are directed against the relapsing-remitting form of MS. Therapy for this type of MS includes immunotherapy medications such as interferon-beta 1 (IFN-β1) and glatiramer acetate. Clinical studies by Jacobs and Li have demonstrated reduced onslaught of MS symptoms when treatment with IFN-β1 is started at disease onset (30). IFN-β1 is known to inhibit immune cells from crossing the blood-brain barrier (30,31). Glatiramer acetate inhibits T helper lymphocytes from influencing neighbouring immune cells in MS (32,33) and if administered in early CIS, it reduces relapse and new lesion development in 33% of patients without side effects (34–36). However, there is no significant difference between IFN-β1 and glatiramer acetate in terms of relapse outcome and neither of these treatments completely inhibit the progression of MS in all patients (37). Immunotherapy medications such as IFN-ß1 and glatiramer acetate are not permanent therapies, however, recent drug trials are determining future treatments.

A more recent medication verified for MS treatment includes natalizumab. Natalizumab, a monoclonal antibody specific for adhesion integrin alpha-4, is currently used in MS treatment to prevent the adhesion of inflammatory cells to the blood-brain barrier and gut wall, hence inhibiting the binding and entry of inflammatory cells into the CNS (38). Interestingly, a single case study by Sera and colleagues has shown that when natalizumab therapy was ceased there was a case of severe MS disease relapse to the point of mortality, with a huge influx of EBV-infected B lymphocytes in lesions in the CNS of the patient, which was analysed post-mortem (38). This disease relapse post-natalizumab has occurred before and it was further hypothesized that the use of B lymphocyte depletion

therapy post-natalizumab treatment would be beneficial (38,39). B lymphocyte depletion therapy has been further investigated in clinical trials.

3.4.1 B lymphocyte depletion therapy for MS

B lymphocyte depletion therapy has been successfully used in autoimmune diseases including rheumatoid arthritis, lupus, Sjogren's syndrome, and more recently, these drugs were tested on patients with MS. In the first clinical trials (phase II and III) (40,41), B lymphocyte depletion therapy using rituximab, ocrelizumab and ofatumumab have shown a promising effect in reducing the risk of MS relapse by decreasing inflammation. These three therapies are all monoclonal antibodies shown to successfully target B lymphocyte surface antigen $CD20^{+}$ through different mechanisms of action, hence depleting B lymphocytes. A study by Palanichamy et al. discovered MS patients undergoing rituximab therapy had a significant reduction in B lymphocytes for more than 6 months (42). A further study detected decreased B lymphocyte markers in the CNS in MS patients (40). In animal models of multiple sclerosis, the disease progression was significantly reduced by the elimination of interleukin-6 (IL-6)-producing B lymphocytes, which coincided with the reduction in myelin antigen-specific helper Th1 and Th17 lymphocytes (43,44). In randomized double-blind, placebo-controlled trials, where patients were treated exclusively with rituximab after switching from other first-line injectable therapies, there were reduced CNS lesions by 24 weeks, especially in younger patients (41,45,46). These studies are evidence for a potential future MS treatment in B lymphocyte depletion therapy and highlights the need for focused research into B lymphocytes in the context of MS.

4 Aetiology of MS

MS is an autoimmune disease characterized by the immune system attacking the myelin sheath of the CNS, however, the exact aetiology of this autoimmune attack in MS is unclear. Like for other autoimmune diseases, including lupus and rheumatoid arthritis, there is evidence in MS for a genetic predisposition and influence of environmental risk factors (47–49). The most documented MS risk in the disease susceptibility gene on the human leukocyte antigen (HLA) DR (42,44), and in particular HLA-DRB1*1501, significantly increase the risk of developing MS. There is also a link between gender and autoimmune disease, where women are more susceptible to MS than men(52,53).While many environmental risk factors for MS have been described, including smoking (47), diet (54,55) and air pollution (56), the most significant environmental risk for MS in multiple studies include Vitamin D deficiency (48) and EBV infection (57).

4.1 MS demographics

There is evidence that individuals in countries with greater latitude are at increased risk of developing MS, which has been mainly attributed to lower exposure to sunshine and therefore, lower Vitamin D levels in individuals further away from the equator. The first association of MS and latitude was described as early as 1921 (58). According to the Atlas of MS 2013 data, countries distant from the equator, such as the United States of America, Russia, Germany and United Kingdom, have the highest number of people living with MS: 400,000, 150,000, 130,000 and 100,000 respectively (59) (Figure 8.1), but population densities were not given in this investigation. In Australia alone, 21,283 people are living with MS (59) while Asian and African countries show the lowest number of people with MS which might be partially skewed by insufficient data reporting. Of note is the effect of latitude on MS, which is also observable across Australia. There are high numbers of MS patients in Tasmania, compared to Perth and Melbourne with

lowest incidences of MS in Northern Queensland (60). Data for Europe is typically aligned with this theory of latitude risk, such as Ireland, which has a higher incidence rate than the rest of the British Isles, according to a recent 292 patient study (61). However, an exception to the theory of latitude risk is Norway, where there are very low incidences of MS despite its latitude (62), which has been mainly attributed to a high Vitamin D intake with the diet (62). Of note, the effect of latitude seems to be true for early childhood exposure up to the age of 15, as shown in migration studies (63). Overall, MS is linked to latitude with the exception of nations where dietary consumption of Vitamin D is high.

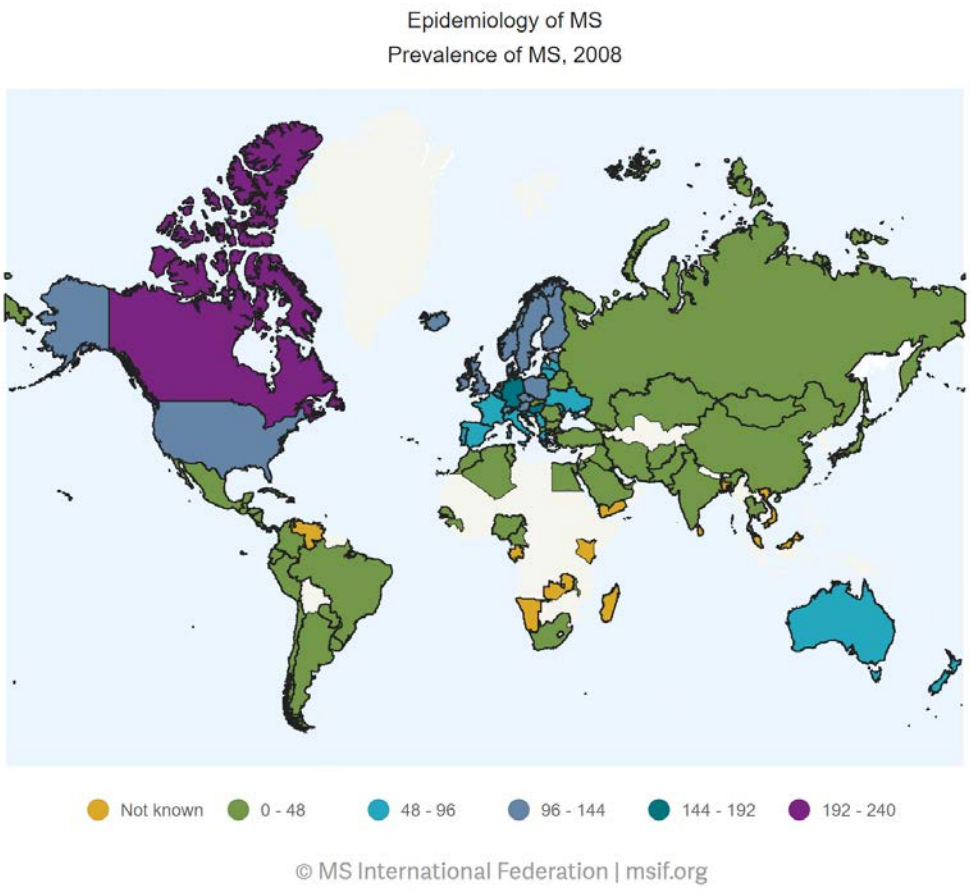

Figure 4.1: Global prevalence of MS. The greatest prevalence of MS is in developed countries such as Canada, Europe and the United States. The lowest known prevalence is in developing countries near the equator such as Russia, Middle East, Asia and South Americas (59). *Image from Atlas of MS 2008 MS International Federation.*

4.2 Genetic susceptibility to MS

4.2.1 Human leukocyte antigen (HLA) alleles

The human leukocyte antigen (HLA) is positioned on the surface of immune cells such as T and B lymphocytes. HLA Class I is located on the surface of all nucleated cells and HLA Class II is mainly situated on the surface of antigen-presenting cells (APCs), functioning in the processing of antigens and presenting them to T lymphocytes. The main genetic risk factor for MS susceptibility has been found in genome-wide association studies (64) to be HLA-DRB1*1501. This variant has been discovered to be significantly more present in MS patients than healthy controls in several studies from different countries including US, Australia and Europe (65). The allele frequency of this risk allele in MS may be a result of epigenetics that are affected by maternal origin, generational differences, sex-specific mechanisms and external environmental factors (66). The combination of EBV and HLA-DRB1*1501, or on their own, are known to increase the risk of developing MS (13,85). Due to structural similarities, HLA-DRB1*1501 on T lymphocytes recognise myelin basic protein (MBP) and EBV peptides such as EBV DNA polymerase in the CSF of MS patients (67,68). There are multiple potential cross-reactive targets identified to include HLADRB1*15-restricted epitopes, myelin and paranodal assembly proteins, all of which may be novel myelin antigens targeted by $CD4^+$ T lymphocytes in MS patients (69). The targeting by the immune system of self-antigens, such as myelin, is called autoimmunity and may be due to molecular mimicry.

4.3 Molecular mimicry

Molecular mimicry occurs when a small protein (peptide) of a foreign molecule resembles a self-antigen, and hence cross-reactivity can occur. This hypothesis has now been confirmed by multiple studies, directly linking different EBV proteins, such as EBV nuclear antigen- 1 (EBNA-1), with MS through autoreactive targets in the CNS (8–10).

Prior to EBV infection, auto-reactive B lymphocytes in the bone marrow normally undergo deletion, however, during autoimmune disease this control breaks down and auto-reactive B lymphocytes clonally expand (70). In MS, molecular mimicry involves EBV, auto-reactive B lymphocytes that produce cross-reactive antibodies, and self-myelin antigens such as those antibodies that have specificity for either myelin basic protein (MBP), myelin oligodendrocyte glycoprotein or proteolipid protein (10). EBV proteins have been shown by Lünemann, et al., to structurally mimic MBP and subsequently, the MBP is marked as a target antigen for T lymphocytes (8). These mimic EBV antigens may be expressed by EBV-infected autoimmune B lymphocytes as they clonally expand and migrate towards the CNS, where it is theorized that they pass the blood-brain barrier as B lymphocytes have been shown in the past to be present in MS lesions in the CNS (71,72). Clonally-expanded EBV antigen-specific T-helper lymphocytes and memory T lymphocytes may also contribute to MS by cross-recognition of self-antigens, such as myelin antigens, or by T cell receptor-independent bystander mechanisms (9,73,74). These $CD4^+$ T lymphocytes may migrate to the CNS, attracted by cytokines released by autoreactive B lymphocytes existing in the CNS, and interact via MHC class II as the B lymphocyte presents the myelin self-antigens and expresses co-stimulatory molecules (75–77). An investigation by Casiraghi, et al., presented evidence of the co-stimulation of T lymphocyte marker $CD40^+$ causing an upregulation of $CD4^+$ and $CD8^+$ effector T cells in an animal model for MS during EBV latency, whilst there was a downregulation of suppressor T regulatory (T_{reg}) lymphocytes (78). This is clear evidence of increasing autoimmune reactivity (78) to EBV proteins and $CD8^+$ response in MS patients (79). These increased inflammatory cells are attracted to the CNS and attack the myelin, causing demyelination and damage to the neuronal function. Whilst the risks of molecular mimicry in MS in relation to EBV are quite high, there is evidence that this factor does not act alone for MS to develop.

4.4 Epstein-Barr virus as a risk factor for MS

4.4.1 Introduction to EBV

EBV is a DNA virus belonging to the human herpesvirus (HHV) group, in which it is denoted as HHV-4. It has evolved alongside humans for millions of years. EBV, like other human herpes viruses, has a large and complex genome. The virus is comprised of double-stranded DNA encased in a nucleocapsid. Outside the nucleocapsid is the tegument, which is analogous to the matrix in other viruses. The tegument itself is surrounded by a lipid bilayer envelope which is embedded with glycoproteins such as gp350, gB, gH and gL enabling the virus to penetrate B lymphocytes (80,81).

Approximately 90% of the human population is infected with EBV but primary infection rarely causes severe symptoms. In contrast, the primary infection can cause severe symptoms which then present as infectious mononucleosis or glandular fever. Mostly, EBV exists latently in humans and is transmitted via saliva, typically during early childhood or intimacy between adolescents. There is some evidence that EBV uses mechanisms during lytic phase to avoid the immune system prior to entering latency, including the inhibition of monocyte phagocytosis (82) and compromising T lymphocyte antiviral responses through precursor dendritic cell apoptosis (83), enabling it to persist. This persistence and effect on the immune system may lead EBV to be a key trigger of multiple autoimmune diseases such as MS, systemic lupus erythematosus and rheumatoid arthritis (84,85).

4.4.2 EBV and MS

4.4.2.1 EBV antibody titres in MS patients

EBV infection has been implicated to have a strong correlation with MS. The presence of high antibody activity specific for EBV has been detected in CSF and blood sample testing from MS patients in multiple studies (79,86,87). A study by Cepok, et al. observed significantly higher antibodies specific for EBV proteins EBNA-1 and BRRF2 in the CSF and serum of MS patients compared to controls (79). These results were also confirmed by two other groups for EBV antibodies in both serum and CSF (86,87). A single controversial study by Serafini and colleagues discerned MS patients' brain tissues were infected with EBV (88). However, there were limitations to this study as they only investigated a small sample of 22 people, leading to controversy when peer reviewed (89) as no other group could replicate direct presence of EBV in postmortem samples. Despite this, there have been studies to show the reactivation of EBV into the lytic stage in MS patients, as compared to healthy EBV-seropositive individuals by EBV protein studies and MRI scans of the CNS for demyelination (90–92). EBV is a significant factor in MS aetiology and may be the key trigger of this disease.

4.4.2.2 Oligoclonal Bands

There is further evidence for a link between MS and EBV with the testing of CSF for increased levels of IgG protein during diagnostics. This protein forms oligoclonal bands, which are the only clinical biomarker currently used for MS diagnosis. IgG in MS patients has been found in some studies to be specific for EBER, however, this is not always the case, with low specificity in other research and equivalent specificity to other non-MS neurological diseases (6,7).

Oligoclonal bands are produced by B lymphocytes, which is indicative of an inflammatory response in the CSF. The presence of the oligoclonal bands is telling of the

clonal expansion of B lymphocytes that occurs in the CSF; and as it is known that B lymphocytes undergo somatic hypermutation and class switching recombination when they are latently infected with EBV (87,93). It is theorized these B lymphocytes release antibodies with high affinity for the antigen in a process called affinity maturation, which leads to elevated levels of IgG and complement deposits in lesions.

4.4.2.3 Infectious Mononucleosis and MS onset

Infective mononucleosis (IM), the illness that arises due to infection with EBV, is significantly associated with MS development, as infection with EBV in older people often leads to symptoms presenting in IM and increases the risk of MS by about 2.3 fold (65) This illness can be catastrophic in immunosuppressed patients but is typically asymptomatic and harmless in healthy individuals. Symptoms of IM are characterized by fever, sore throat and swollen lymph nodes (94). These symptoms are caused by the inflammatory response of the 1-40% of $CD8^+$ T lymphocytes specific for EBV antigen and the 10% of B lymphocytes that are infected with EBV virions (95). IM is a self-limiting disease and symptoms rarely persist (94). However, it is hypothesised that there is a window of time during childhood when EBV infection occurs and MS subsequently may occur during a later stage of life (4). In multiple studies, MS patients from various countries were asked to recall their age when they had IM and it was shown that if infection occurred between puberty and the age of 18, the risk of developing MS increased (5,96). It is important to note that recollection of past events by patients can be subjective, especially as IM symptoms could be mistaken for a cold or flu. Nonetheless, there is significant evidence for a link between the age of EBV infection and MS development.

5 EBV and the immune system

5.1.1 T lymphocyte responses against EBV

T lymphocytes have been a major focus of research into the complex immunological relationship between EBV and MS. It is theorized that $CD8^+$ T lymphocytes are defective in their control of proliferating EBV-infected auto-reactive B lymphocytes. A study by Pender completed this year confirmed that defective $CD8^+$ T lymphocytes may be the reason why B lymphocytes latently infected with EBV are able to clonally expand into an autoreactive population in MS patients (97). Pender and colleagues had already demonstrated in an earlier study that a deficiency in $CD8^+$ T lymphocytes is persistent in MS patients, which would explain the impaired control of infected B lymphocytes (98). Nevertheless, a study last year by van Nierop, et al., has revealed there is no evidence of intrathecal $CD8^+$ or $CD4^+$ T lymphocyte reactivity to MS self-antigens after the onset of disease and there are currently no studies on the reactivity of T lymphocytes to MS antigens prior to the onset of disease (99). However, van Nierop, et al., also determined in another study that intrathecal $CD8^+$ T lymphocytes of MS patients recognise lytic EBV proteins (100), proving a direct link between T lymphocytes and EBV. Whilst T lymphocytes have been prominent in research into the link between MS and EBV, B lymphocytes are also a major focus, as they are the carriers of EBV.

5.1.2 Acute EBV infection of B lymphocytes

EBV infection mechanisms in healthy human carriers begin with primary infection of circulating naive B lymphocytes in the oropharynx and the epithelial cells of the tonsils, as shown in Figure 5.1. EBV gains entry to the cell by the binding of the glycoprotein gp350 to the cell surface complement receptor 2 (CR2), the most common glycoprotein on its surface, as well as the aid of other glycoproteins (81). EBV replicates in the B

lymphocytes and causes clonal transformation. Typically, the immune system is primed by memory T lymphocytes to reactivate EBV-specific cytotoxic $CD8^+$ T lymphocytes, which control the growth of EBV-transformed B lymphocytes, but are prevented from attacking EBV-infected resting B lymphocytes, enabling persistent infection (101). These latently infected memory B lymphocytes move to tonsil lymphoid tissue and then the blood and other lymphoid tissue to exist in dissemination. Subsequently, the infected memory B lymphocyte persistence is lifelong in the individual. During acute infection, when the EBV is reaching the maturation phase, it adjusts the structure of the nuclear membrane of immune cells to allow lytic reproduction (102). Lytic infection is characterized by EBV replication in the B lymphocytes and subsequent cell lysis with virion release. Released virions can infect more B lymphocytes and epithelial cells, enabling shedding of EBV in saliva and blood (101). This shedding of EBV is what enables transmission of the virus between individuals via saliva, allowing the virions to spread.

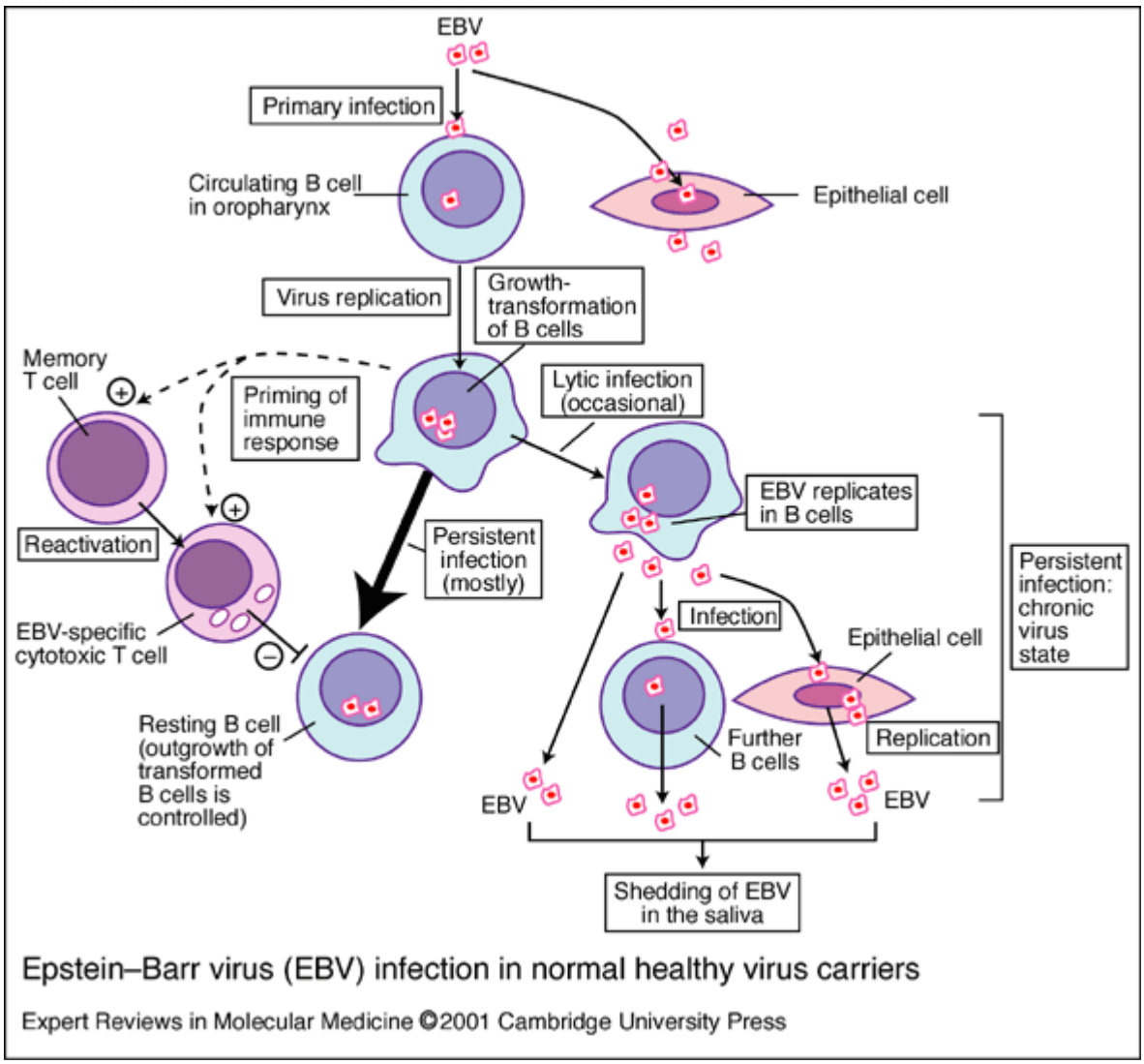

Figure 5.1. Acute and latent EBV infection mechanisms in normal healthy individuals (101). The EBV virion infects B lymphocytes and epithelial cells in the oropharynx. The virus subsequently uses the B lymphocytes as tools of replication and causes clonal expansion. During lytic infection, the EBV virions burst the cell membrane, entering the lymph gland environment to infect more B lymphocytes and replicate again. The released virions can be passed on to other individuals through saliva (101). The immune response of T lymphocytes inhibits excessive expansion of the infected B lymphocytes however some EBV cells persist in memory B lymphocytes and enter latency (*Image taken from Expert Reviews in Molecular Medicine 2001 Cambridge University Press.).*

5.1.3 Latent EBV infection of B lymphocytes

Latent EBV will persist in the human body for the individual's lifetime. EBV can be reactivated in B lymphocytes if the immune system is compromised and enter the lytic stage again. In rare cases, EBV can cause tumorigenesis and cancerous development such as Burkitt's lymphoma, nasopharyngeal carcinomas, oral leukoplakia with higher prevalence in low socio-economic countries (103). In the case of MS, it is theorised that EBV-infected memory B lymphocytes interact with APCs, such as dendritic cells, during latency and cause a skewed Th1 autoimmune response against the myelin sheath of the CNS (70). This may be how the virus is able to hide from the immune system during the three stages of latency, I, II and III (104). These stages are characterized by the initiation of mitosis of infected memory B lymphocytes and creation of a germinal centre to persist in and clonal expansion respectively (104).

5.2 EBV gene expression

In latency, EBV genes express proteins that can aid in the persistence of the virus within B lymphocytes. These include Epstein-Barr virus Nuclear Antigen 1 (EBNA-1), Epstein-Barr virus-encoded small RNAs (EBER), Latent Membrane Protein 1 and 2 (LMP1 and LMP2). EBNA-1 is expressed throughout the virus lifecycle, including latency and lytic stages, and functions in the suppression of viral reactivation as well as the disruption of promyelocytic leukaemia nuclear bodies of infected cells in order to initiate the cell lysis cascade (105). Latency II and III phases both have the presence of LMP1 and LMP2, which are viral membrane proteins indirectly transactivated by EBNA-1 (94). EBNA-1 is of major importance to the virus as in order to ensure duplication of the viral genome during mitosis, it attaches the viral episome to the host genomic DNA. (105). Additionally, EBV cannot reactivate without the essential EBNA-1 gene positively

affecting its own synthesis through a latently-active promotor, as shown in studies (106). LMP, an important component of the membrane, enables the EBV-mediated transformation of cells (107). The role of EBER, a highly expressed RNA with no gene product, is unclear, however, it has been theorized that it is involved with the oncogenic activity of the virus due to its ability to confer resistance to apoptosis, increase in tumorigenicity of the virus and induction of growth factor production (108). The constant latent expression of EBNA-1 and EBER make them ideal targets for quantification of EBV viral load.

6 EBV detection

Researchers have previously detected EBV in lytic and latent infection using various methods including serology testing, DNA analysis and in situ cellular studies. The link between MS and EBV has previously been studied due to the presence of high EBV-specific antibody titres (50) in MS patients, as produced by B lymphocytes that have converted into plasmablasts. These antibodies were detected for serology by enzyme-linked immunosorbent assay (ELISA) (50). However, B lymphocytes have been known to act as APCs (70) and hence it is important to determine if EBV-infected B lymphocytes are related to autoimmunity in EBV latency by detecting latent EBV genome copy numbers. There have been various methods used to detect EBV in lytic infection, either during acute initial infection or reactivation of the virus. Often, reactivation of the virus can lead to tumorigenesis of cells where tumours can develop, such as Burkitt's lymphoma and nasopharyngeal carcinoma (103). For the purpose of creating an EBV-infected cell line, single cells containing EBV have been extracted from tumours and expanded for analysis of EBV in the past (109). Incidentally, methods have been developed to detect EBV within these cell lines where there are high copy numbers of the EBV genome. A commonly used technique is *in situ* hybridisation, which has been in use for EBV detection since 1996 (110). This method has successfully determined EBV infection in both lytic and latent states, using a large DNA probe of 14.7kb specific for *Bam*HI, a fragment of the EBV genome, to detect from as little as eight EBV genomes to 200 EBV genomes per 10^5 PBMCs (111). However, it is difficult to accurately quantitate DNA copies using this technique due to the need for manual counting, as opposed to automated counting in other more recent methods.

Alternatively, a technique of particular note is the use of quantitative reverse-transcription polymerase chain reaction (qRT-PCR) for automated quantification of lytic EBV RNA transcripts. This method requires a standard curve to be developed using serial dilutions of the target to allow comparison for quantification. Though the low viral load during the phases of latency makes detection of EBV difficult, the constant expression of EBNA-1 and EBER in latency can aid in detection. EBNA-1 is difficult to detect due its glycine-alanine rich region, which cross-binds with host genomic DNA during PCR methods (69) Hence, a technique to eliminate the presence of genomic DNA is needed, such as qRT-PCR, where the initial sample is RNA converted into cDNA (112). qRT-PCR has been used for lytic EBV quantification in multiple studies of EBV-infected cell lines (112,113), however, qRT-PCR has only quantitated EBV in latency in two studies (114,115), with a detection limit as low as 16 copies/mL of EBNA-1. Only one of these qRT-PCR studies, by Cocuzza and colleagues, was commenced in the context of MS and there was found to be no significant difference in EBNA-1 copy numbers in CSF and whole blood between relapsing-remitting MS and healthy controls (115). However, it was noted that the method of RNA extraction was not consistent with other studies (115). qRT-PCR can be used for detection of EBV in lytic infection, however, this technique needs to be tested further in latent infection.

A recently available method of quantification is digital droplet polymerase chain reaction (ddPCR). Oil droplets are utilized in this technique to separate the DNA strands for automated quantification. ddPCR has been successfully used for EBV detection in high viral load samples by Vo, et al., who quantified lytic EBV in whole blood in the context of nasopharyngeal analysis (116), with a minimum limit of detection verified to be 9 DNA copies/mL. Other viruses, such as human immunodeficiency virus (HIV), were previously detected in latency using ddPCR, which the group compared to qPCR results for the same samples. Trypsteen, et al. did not find a significant difference between the

two methods (117). ddPCR has so far not been used to quantify latent EBV when very low copy numbers are expected.

A technique called flow cytometry couples with fluorescent in situ hybridisation (Flow-FISH) was used to detect EBV-transformed cell lines from Burkitt's lymphoma tissue and peripheral blood from patients with lymphoproliferative disease. One study, by Kimura and colleagues, used a peptide nucleic acid (PNA) probe specific for EBER for EBV identification by flow cytometry for determination of EBV in lymphoproliferative diseases (118). This assay successfully determined lymphocyte infection with lytic EBV (118), however, the technique has not yet been used for latent EBV PBMC infection analysis. A second study used the same EBER PNA probe for characterization of EBV-transformed cell lines Raji, Daudi and HS-Sultan to determine the suitability of this probe for flow cytometry analysis (119). The probe was concluded to be appropriate for the flow-FISH analysis of EBV-infected cells.

7 B lymphocytes and MS

7.1 B lymphocytes in the central nervous system

B lymphocytes have previously been considered secondary to T lymphocytes in terms of finding a clinical target for MS. While evidence demonstrates that T lymphocytes recognise self-antigens due to EBV in MS, there is data to indicate that B lymphocytes produce antibodies specific for self-antigen (74). A number of studies give evidence for the changes of B lymphocytes behaviour during MS disease, such as detectable increased presence in the CNS in MS, however, this is heavily disputed (120,121,1).

The presence of B lymphocyte follicle-like structures in the subarachnoid space of the CNS in MS have demonstrated increasing demyelination in one study (121). Krumbholz and colleagues discovered that in MS, an environment can be created in these follicle structures that enable the further development of B lymphocytes, as determined by the presence of B lymphocyte-activated factor of the TNF family factor, a proliferation-inducing ligand and plasma cell survival factor (122). This increases B lymphocyte expansion (122). This may be evidence for an environment in the CNS of MS patients that allows the expansion of B lymphocytes.

EBV-infected B lymphocytes were used as APCs in a study and there was confirmed to be significant T lymphocyte reactivity in the CNS in the presence of lytic EBV proteins (100). This is a result of dysregulation of B lymphocytes by EBV, which can be discerned in white lesions in the CNS of MS patients at all stages of the disease according to one study (88). By analysis of post-mortem MS brain tissue in a 2010 study, there appeared to be EBV deposits with lesions comprising $CD27^+$ T lymphocytes along with the presence of survival and maturation signals for B lymphocytes (3). Possibly pathogenic memory B lymphocytes have been identified in MS, including CD22, CD24, CD25,

CD27, CD49d, CD83, CD180, $CD38^{low}$, HLA-DR, CCR2 CCR6 (120), however, there is yet to be studies into the relationship between these pathogenic B lymphocytes and EBV. More recently, the levels of EBNA-1 antibodies have been proven to be higher in the serum (69) of MS patients than controls and CSF or both, hence making peripheral blood an excellent source for sampling levels in MS patients as opposed to CSF via the lumbar puncture, which is a current diagnostic measure (123). Peripheral blood would be a suitable sample for testing both EBV and B lymphocytes simultaneously.

8 Study rationale

The complex relationship between EBV, MS and the immune system, particularly B lymphocytes, requires further focussed research. EBV has been implicated in MS, as evident in high antibody titres specific for EBV in peripheral blood in MS patients compared to healthy controls (50). Further evidence for this association is the high EBV specific oligoclonal bands in the CSF of MS patients, not found in controls (7). Additionally, the linkage between MS and EBV infection is further supported by the increased risk of MS disease when individuals had symptomatic EBV infection and presented with infectious mononucleosis. Moreover, previous studies have linked the significance of EBV as a key trigger for MS in conjunction with other risk factors such as Vitamin D and HLA loci and how B lymphocytes are involved in EBV in humoral immune response.

The role of T lymphocytes was initially always the main focus of MS research (69) into the relationship between EBV and MS, however, the role of EBV-infected B lymphocytes has quickly become of interest due to their role as APCs (70). More recently, the significance of B lymphocytes has become apparent in the results of B lymphocyte depletion therapy in MS patients as the absence of B lymphocytes significantly reduced MS remission and symptoms (45,46). Whilst EBV is known to reside within B lymphocytes in latency, it is unknown if the amount of EBV within different B lymphocyte subsets varies between MS patients and healthy controls and if these infected cells are more likely to develop into plasma cells, produce cross-reactivity producing antibodies or serve as APCs.

The detection of EBV in latency has proven difficult due to poor sensitivity for low viral genome copy numbers. However, the technique of FISH has been used with flow cytometry to detect EBER expressed by EBV in latency for EBV detection method

development within infected cells in a single study of infected peripheral lymphocyte subtypes, but not in MS (118). This technique does not allow the accurate quantification of EBV due to the need for manual counting. However, some automated techniques, such as ddPCR and qPCR, have been used in single studies to quantitate the latently expressed EBNA-1 at low levels of 10 copies/mL and 16 copies/mL respectively (116,124). These techniques are yet to be replicated and they have not yet been used for EBV in the context of MS.

Once EBV can be reliably detected in latency, the functional properties of EBV-infected B lymphocytes in MS can be defined. This will contribute to research into new biomarkers in the disease and ultimately lead to improvement of the quality of life for MS patients, earlier MS diagnosis and more specific and targeted treatment.

9 Hypothesis and aims

In this study, a method for EBV quantification in B lymphocytes in MS patients and healthy controls will be used to determine which B lymphocytes are latently EBV infected and if there is a significant difference in EBV genome copy numbers between different B lymphocytes subsets in MS patients in comparison to healthy controls. qPCR and ddPCR have been shown in other studies to be highly sensitive quantitative methods. In this project, they will be utilized to detect EBNA-1, a latently expressed gene. To determine the ratio between the different B lymphocyte subsets, B lymphocytes will be isolated by negative selection. In a third quantification method, Flow-FISH will be used to target EBER, a highly expressed EBV RNA in latency, to identify EBER positive B lymphocyte subsets in flow cytometry. These techniques are proposed to allow the quantification of EBV at very low levels in latency in MS patients and healthy controls.

We hypothesize that i) it is important to gain knowledge about EBV copy numbers in B lymphocyte subsets and that ii) the comparison between ddPCR, qPCR and flow-FISH will inform about the best suitable method for sensitive and specific EBV quantification in B lymphocytes. iii) Using the combination of sensitive EBV quantification will elucidate EBV copy numbers in B lymphocytes subsets. By defining specific EBV-containing B lymphocyte subsets, this research may provide valuable guidelines for MS therapy by targeting B lymphocyte depletion therapy more specifically for a subset of B lymphocytes only, limiting side effects and improving quality of life; and prove useful as a biomarker if results show different quantities of EBV in B lymphocytes between MS and healthy controls and could aid in diagnosing MS patients before initial symptoms occur.

10 Materials

10.1 List of kits

Kit	Use	Manufacturer
RNeasy Plus RNA Extraction Kit	RNA extraction	QIAGEN, AU
ddPCR EvaGreen Kit	ddPCR analysis	Bio-Rad, AU
qPCR EBV ASR Probe/Primer Kit	qPCR analysis	QIAGEN, US
EasySep Human B Cell Isolation Kit	B lymphocyte enrichment	Stem Cell Technologies, AU

10.2 List of reagents

Reagent	Manufacturer
Whole blood processing	
Ficoll	Bovogen, AU
10% dimethyl sulfoxide (DMSO)	Bovogen, AU
Fetal Calf Serum (FCS)	Bovogen, AU
Phosphate Buffered Saline (PBS)	Bovogen, AU
Vi-Cell Lysis Buffer	Invitrogen, AU
RNA extraction	
β-Mercaptoethanol	Invitrogen, AU

Ethanol Absolute	AJAX, AU
DNase I	QIAGEN, AU
DNase Buffer	QIAGEN, AU
RNase OUT	Invitrogen, AU
HLA-C PCR	
TDMH-B Buffer	Sigma-Aldrich, AU
GoTaq Polymerase Enzyme	Promega, AU
Agarose gel electrophoresis	
UltraPure Agarose Powder	Invitrogen, AU
UltraPure Ethidium Bromide	Invitrogen, AU
TAE	Sigma-Aldrich, AU
cDNA reverse transcription	
5x First Round Buffer	Invitrogen, AU
10mM dNTPs	Invitrogen, AU
DTT	Invitrogen, AU
RNase OUT	Invitrogen, AU
SuperScript III Reverse Transcriptase	Invitrogen, AU
Oligo dT (100pmol/µL)	Invitrogen, AU

qPCR analysis	
iTaq Universal Probes Supermix	Bio-Rad, AU
B lymphocyte enrichment	
PBS	Bovogen, AU
EDTA	Sigma-Aldrich, AU
Flow-FISH analysis	
Glacial Acetic Acid	Sigma-Aldrich, AU
Paraformaldehyde	Sigma-Aldrich, AU
Tween 20	Sigma-Aldrich, AU
Sodium Chloride	Sigma-Aldrich, AU
Disodium EDTA	Sigma-Aldrich, AU
Tris-Hydrochloric Acid	Sigma-Aldrich, AU
Formamide	Sigma-Aldrich, AU
Y5200 EBER PNA Probe	DAKO, US

10.3 List of antibodies for flow-FISH analysis

Antibody	Manufacturer
BD Pharmingen Mouse Anti-Human CD19 PE Antibody	BD Biosciences, AU
BD Horizon Mouse Anti-Human CD24 PE-CF594 Antibody	BD Biosciences, AU
BD Horizon Mouse Anti-Human IgD Pe-Cy7 Antibody	BD Biosciences, AU

BD Horizon Mouse Anti-Human CD20 APC-H7 Antibody	BD Biosciences, AU
BD Horizon Mouse Anti-Human CD38 BV421 Antibody	BD Biosciences, AU

10.4 List of primers

Primer	Target	Use	Manufacturer
EBV forward/reverse primers	97bp EBNA-1	qPCR	QIAGEN, US
M13 forward primer	5'-GTAAAACG ACGGCCAGT-3'	EBNA-1 standard	Integrated DNA Technologies, AU
M13 reverse primer	5'-AACAGCTA TGACCATG-3'	EBNA-1 standard	Integrated DNA Technologies, AU
HLA-C forward/reverse primers	HLA-C	HLA-C PCR	Integrated DNA Technologies, AU
ddPCR forward primer EBNA-1 109111*	5’TCATCATCATCCG GGTCTCCACCGC3’	ddPCR	Integrated DNA Technologies, AU
ddPCR reverse primer EBNA-1 109951*	3’CAACAGCACGCA TGATGTCT5’	ddPCR	Integrated DNA Technologies, AU

*The ddPCR primers were developed by Dr Monika Tschochner, Institute for Immunology and Infectious Diseases.

11 Methods

11.1 Collection and processing of healthy control blood samples

38 peripheral blood samples were collected from healthy control patients from the Australian Red Cross and Murdoch University Clinic using vacutainer tubes with EDTA. Blood was diluted with RPMI, then overlayed on Ficoll and centrifuged for separation of peripheral blood monocytes (PBMCs). PBMCs were frozen at 10 million cells in 800µL with 10% dimethyl sulfoxide (DMSO) in fetal calf serum (FCS) in liquid nitrogen at -80^{o}C for future testing. When needed, cells were thawed and washed twice with PBS by centrifugation and rested overnight in an incubator for 12-18 hours in 5mL of R10 at 37^{o}C at 5% CO_2.

After resting, the PBMCs were resuspended in 10mL PBS and counted in the Vi-Cell counter (Invitrogen, AU) using 540µL of cell lysis buffer and 60µL of sample. PBMCs were then centrifuged again and resuspended in the required amount of media or buffer as per protocol for either flow cytometry, qPCR or ddPCR experiments.

11.2 Extraction of RNA from PBMCs for quantification

RNA was extracted using the commercial RNeasy Plus kit (QIAGEN, AU). RNA samples were kept on ice to reduce RNase activity. RNA extraction was performed according to manufacturer's instructions but as a slight variation, genomic DNA was digested twice with DNase I to reduce non-specific amplification. Briefly, this involved the preparation of Buffer RLT Plus by adding 20µL β-mercaptoethanol (β-ME). To disrupt the pelleted cells, Buffer RLT plus and 70% ethanol was added to the sample. The sample was added to the RNeasy spin column membrane in a collection tube and centrifuged. Buffer RW1 was added to the spin column and again centrifuged. The flow-through was discarded but the collection tube and spin column were retained. 100µL of 1:10 DNase I in buffer was

added to each sample. This was incubated with the sample in the spin column at room temperature for 30 minutes, instead of the 15 minutes recommended by the manufacturer. Buffer RW1 was again added and centrifuged. This was repeated with Buffer RPE. This wash step was repeated once more with centrifugation for 2 minutes. The spin column was placed into a fresh collection tube.

To enable elution of the purified RNA, 30µL of RNase-free water was added to the column membrane and the sample was eluted into the collection tube after centrifugation. The RNA was stored at aliquots of 10µL at -80^{o}C with 1µL of RNaseOUT to reduce RNase activity. Nucleic acid concentration from each sample was analysed after extraction by spectrophotometry using Nanodrop. Each RNA sample was gel electrophoresed with 1µL per sample on a 1% agarose gel stained with ethidium bromide to confirm extraction. The gel was electrophoresed for 30 minutes at 110 volts.

11.3 Use of HLA-C PCR for confirmation of RNA purity

To determine if there is a significant amount of DNA present in the RNA sample after extraction, an in-house HLA-C PCR was performed. The primers (Integrated DNA Technologies Inc) were designed to amplify both DNA and RNA but would result in different lengths of 3Kbp and 1Kbp amplicons, respectively. PCR conditions are shown in Table 11.1.

Temperature	Time	
96°C	6 minutes	
96°C	30 seconds	
62°C	30 seconds	Repeat for 35 cycles
72°C	2 minutes	
72°C	10 minutes	
4°C	Forever	

Table 11.1 Thermocycling conditions for the HLA-C PCR. The PCR allows for amplification of DNA and RNA in samples resulting in different fragment sizes of 3Kbp and 1Kbp, respectively.

11.4 cDNA conversion of RNA

RNA was reverse-transcribed into complementary DNA (cDNA) using oligo dT, which are short sequences of deoxy-thymidine nucleotides that bind to the poly-A tail of the RNA and result in a free 3' end. This 3' end is extended by the enzyme reverse transcriptase. First, 10µL of each RNA sample were thawed and put on ice where 1µL of oligo dT was added to each sample. A negative control was substituted with 10µL water instead of RNA template. This mix was incubated in a thermocycler for 5 minutes at 65°C and then cooled to 4°C for at least 60 seconds on ice.

The mastermix for the reverse transcription was prepared with 4µL of 5x First Round Buffer (Invitrogen, AU), 1µL of 10mM dNTPs, 1µL 0.5mM DTT (Invitrogen, AU), 0.5µL RNase OUT (Invitrogen, AU) and 0.5µL CSL water. This mix was vortexed and 8µL of the mix was added to each sample. 0.5 µL of Superscript III Reverse Transcriptase (Invitrogen, AU) was added to each sample except the negative control for the enzyme. This mixture was vortexed and then centrifuged for 30 seconds to ensure liquid was at the bottom of the tube. The thermocycler settings for the conversion was 42^{o}C for 60 minutes, 95^{o}C for 3 minutes and then 4^{o}C forever. cDNA was stored at -20^{o}C and freeze-thawing avoided. The maximum number of thawing times for cDNA for downstream assays was set to two times.

11.5 Protocol for digital droplet PCR (ddPCR)

The EBNA-1 cDNA was quantified using a digital droplet PCR (ddPCR) protocol with an oil droplet generator and reader (Bio-Rad, AU). The ddPCR EvaGreen dye (Bio-Rad) mastermix was made up with 12.5µL ddPCR EvaGreen Supermix, 0.1µL forward primer, 0.1µL reverse primer and 9.8µL CSL water to make a total of 22.5µL mastermix per sample. 2.5µL of cDNA sample was added to this mastermix. The EvaGreen dye binds to amplifying DNA and fluoresces.

The primers used were specific for the region of EBNA-1 between positions 109111 and 109951. The positive control used was Daudi, an EBV-transformed cell population from which highly concentrated EBV DNA had been extracted. Two negative controls were used including a negative enzyme control and negative sample control. The 20µL of the sample and mastermix was automatically pipetted into the DG8 cartridge (Bio-Rad) as per the ddPCR droplet generator protocol. 70µL of the EvaGreen droplet oil was also automatically pipetted to the DG8 cartridge within separate wells. A gasket was then

attached across the DG8 cartridge and the cartridge was placed in the QX200 droplet generator. The QX200 was expected to generate ~20,000 droplets/sample in 2.5 minutes for 8 samples. The droplets formed were transferred into a 96 well opaque plate with full skirt slowly using an automated pipette, to avoid disturbance of the droplets or formation of air bubbles. The plate was heat sealed at 170°C with BioRad PX1 PCR plate sealer and pierceable foil heat seal. The thermocycling program was 95°C for 5 minutes then 40 cycles of 95°C for 30 seconds and 60°C for 1 minute, then 4°C for 5 minutes, 90°C for 5 minutes then 10°C forever.

The amplified product was analysed using Bio-Rad ddPCR reader and Quantisoft analysis software (Bio-Rad) which gave the concentration of the sample in DNA copies/µL. Fluorescence of the EvaGreen dye was measured and if it reached the cut-off threshold it was defined as positive, otherwise samples below the threshold were considered negative. The concentration of the samples was calculated by using the proportion of positive and negative droplets and Poisson statistics. The leftover amplified product was alongside a 1Kbp Plus DNA ladder on a 1% agarose gel stained with ethidium bromide and visualised to determine amplicon length. ddPCR amplified products were analysed by Sanger sequencing.

11.6 Protocol for quantitative PCR (qPCR)

11.6.1 EBNA-1 standard development for qPCR

The standard used for qPCR was clonally expanded in a plasmid and was a section of EBNA-1. The plasmid was donated by Anuradha Sooda (IIID) and was isolated by length by electrophoresis on a 1% agarose gel to confirm amplification. The plasmid was restriction digested and the terminal ends of the gene were flanked by M13 primer targets to enable isolation of EBNA-1 by amplification with generic primers. The amplified

product was electrophoresed in agarose gel once more and pooled to enable increased concentration of the product. The product was cut from the gel and purified using spin columns. The purified standard was analysed in triplicate by Nanodrop spectrophotometry for concentration and sequenced using next-generation sequencing as per method used previously by Abha Chopra, et al. (125). The number of DNA copies present in the product was determined by calculation using the results of the Nanodrop analysis.

The standard was serially diluted by 1:10 in Milli-Q water. The serial dilutions, when amplified in qPCR, enabled comparison for quantification of EBNA-1 in samples. Serial dilutions of the standard were tested in all qPCR assays.

A standard curve was generated by plotting log[known EBNA-1 DNA standard copy number] against quantification cycle (Cq) value after qPCR amplification. The Cq value was based on fluorescence of the probe binding to exponentially amplified DNA when crossing the threshold. The slope of the standard curve determined DNA copy number of healthy control samples per 100,000 PBMCs by comparison to initial PBMC counts.

11.6.2 qPCR reaction

The qPCR reaction was set up using a master mix of 200nM forward and reverse primers (QIAGEN US) and 170nM EBV probe (QIAGEN US) with iTaq universal probe supermix 2x (Bio-Rad AU). 2µL of cDNA sample was added to this mastermix for each healthy control and these samples were assayed in triplicate.

The thermocycling conditions of the qPCR were 95^{o}C for 30 seconds for polymerase activation and DNA denaturation, then 60 cycles of denaturation at 95^{o}C for 5 seconds

and annealing/extension and plate read at 60°C for 30 seconds. The fluorescence was analysed by Bio-Rad CFX Manager software (Bio-Rad).

11.6.3 qPCR calculations

The calculation of EBNA-1 DNA copy number was derived from the Cq values of healthy control samples relative to the Cq values of the standard curve. Using the known standard DNA copies against the standard curve Cq values, the healthy control DNA copy number was calculated. The slope of the standard curve was given using the equation:

$$slope=(x_2-x_1)-(y_2-y_1)$$

The number of cycles of standard (Cq value) and $\log_{10}$[standard DNA copy number] were substituted into the equation. The slope value was used to substitute with Cq value for the samples, giving $\log_{10}$[sample DNA copy number]. The inverse log of the healthy control DNA copy number was calculated, and this value was compared to the original cell count taken prior to RNA extraction. To enable relative comparison between samples, the quantity of DNA was given as DNA copy number/100,000 PBMCs.

Amplification efficiency of the qPCR primers and probe were analysed to determine if the 97bp EBNA-1 product was doubled with each amplification cycle. The ideal efficiency would be 100%, with a difference of 3.3 amplification cycles (or Cq value) between 10-fold dilutions of the standard. Amplification efficiency was calculated using a formula from Bio-Rad (126) and the threshold cycle was plotted against the $\log_{10}$[DNA copy number] to the data with a regression line. The amplification efficiency was calculated with the following formula:

$$Amplification\ efficiency = [10(-1/slope)] - 1$$

11.7 Enrichment of B lymphocytes

Copy numbers in EBV latency were expected to be minimal. To enable successful detection, B lymphocytes were enriched for flow-FISH detection of EBER, using a negative selection B lymphocyte isolation kit from Stem Cell Technologies. PBMCs of healthy controls were resuspended to a concentration of 5 x 10^7 cells/mL (0.25 to 2mL) in the recommended medium of PBS containing 2% FCS and 1mM EDTA, which is free from calcium and magnesium ions as per the isolation kit requirements.

The sample was added to a 5mL polystyrene tube and the Cocktail Enhancer (Stem Cell Technologies, AU), which enhances the effects of B lymphocyte enrichment, was added at 50µL/sample. The same amount of Isolation Cocktail (Stem Cell Technologies, AU), which is a combination of monoclonal antibodies in PBS, was also then added, mixed and incubated for 5 minutes at room temperature.

The RapidSpheres (Stem Cell Technologies, AU), which are magnetic particles suspended in water, were vortexed for 30 seconds and added to the samples at 50µL/mL sample and mixed by vortexing. The PBS medium was added to make the sample volume up to 2.5mL and the tube was placed into the EasySep magnet with the lid removed. This mix was incubated for 3 minutes at room temperature. After incubation, the enriched B lymphocytes were poured out of the tube in the magnet into a 5mL fresh tube by inverting for 2-3 seconds without shaking. This new tube replaced the previous one in the magnet for a second separation for 1 minute at room temperature. Once more, the tube was inverted whilst still in the magnet to release the enriched B lymphocytes into another fresh tube. The negatively isolated B lymphocytes were ready to use for flow-FISH.

11.8 Protocol for flow cytometry coupled with fluorescent in situ hybridisation (flow-FISH)

PBMCs only have a very small fraction of B lymphocytes and approximately only 1% of those cells are infected with EBV in latency (70). Fluorescent in situ hybridization coupled with flow cytometry (flow-FISH) gates lymphocyte subsets by surface markers to allow identification of EBV-infected lymphocytes.

Surface antibody incubation and intracellular staining procedure for detection of EBV-positive lymphocytes with an EBER-specific peptide nucleic acid (PNA) probe (DAKO) and flow cytometry. The FITC-labelled probe is specific for EBER RNA. All efforts were made to avoid ribonuclease contamination by using aseptic technique and sterilized equipment.

After overnight resting of PBMCs, cell count and then B lymphocyte enrichment, the cells were incubated with antibodies directed against B lymphocyte surface markers (CD) $CD19^+$, IgD^+, $CD20^+$, $CD38^+$ and $CD27^+$. Using different fluorochrome-coupled antibodies allowed for differentiation between different B lymphocyte subsets in subsequent flow cytometry.

The surface antibody marker panel included anti-CD19, anti-CD24, anti-IgD, anti-CD20, anti-CD38 and anti-CD27, as shown in Table 11.2. Antibodies were incubated with cells were incubated in the dark at 4^oC. Cells were then washed in a buffer containing 1x PBS and 2% FCS and centrifuged at 300 x g for 5 minutes. The supernatant was aspirated and discarded. The cell pellet was used for subsequent fixation and permeabilization for intracellular staining.

Antibody/Probe	Fluorophore	Detector	Volume (µL)	Voltage for B cells (V)	Voltage for LCLs (V)
EBER	FITC	FL1	7	552	410
CD19	PE	FL2	7	500	480
CD24	PE-CF594	FL3	4	436	422
IgD	Pe-Cy7	FL5	4	832	676
CD20	APC-H7	FL8	3	600	577
CD38	BV421	FL9	5	461	368
CD27	BV510	FL10	4	467	343

Table 11.2 List and volumes of surface antibodies used for flow-FISH and the Kaluza (Beckman Coulter) flow cytometer voltage settings used for healthy control B lymphocytes and LCLs. Laser detector channels and fluorophores are included.

Surface marker-stained cells were fixed for 20 minutes at room temperature in a mixture of 4% v/v paraformaldehyde with PBS. To make the fixation mixture, 2g of polymerized paraformaldehyde was added to 50mL PBS and warmed to 60^{o}C whilst pipetting 1M NaOH dropwise (approximately 2mL) to the mixture until the paraformaldehyde dissolved. The solution was returned to a pH of 6.9 by the addition of HCl dropwise (approximately 0.5mL) whilst using a calibrated pH meter (Beckman Coulter). After fixation, the cells were washed twice with PBS/FCS buffer and stored at 4^{o}C in PBS before permeabilization for intracellular staining and tested in flow cytometry within 3 days.

Post-incubation period, the cells were then counted once more and for each sample a total of approximately 5-10 x 10^5 cells were used. These cells were centrifuged at 3500 x g for 5 minutes and then the supernatant was discarded. Permeabilization of the cells prior to

hybridization occurred for 10 minutes in 50 μL 0.5% Tween 20 in PBS at room temperature.

The formamide and buffer concentrations were approximately the same as the hybridization solution, i.e. 31.25mM NaCl, 6.25mM Na2EDTA, 62.5mM Tris-HCl at pH 7.5 and 37.5% formamide. RNase-free water was used to make this mixture.

The EBER probe was initially added at 50μL (DAKO, US) of probe and hybridization solution included with the probe (10% (w/v) dextran sulfate, 10 mM NaCl, 30% (v/v) formamide, 0.1% (w/v) sodium pyrophosphate, 0.2% (w/v) polyvinylpyrrolidone, 0.2% (w/v) Ficoll, 5 mM Na_2EDTA, 50 mM Tris-HCl pH 7.5)). In subsequent testing, the probe was added at 100μL.

The EBER probe was incubated with the B lymphocytes for 60 minutes at 56°C and then 1 mL of 0.5% Tween 20/PBS was added and incubated again for 10 minutes at 56°C. After incubation, the cells were then centrifuged at 3500 x g for 5 minutes and the supernatant was aspirated and discarded. Once more, the cells were incubated for 30 minutes at 56°C with 1 mL of 0.5% Tween 20/PBS and then centrifuged at 3500 x g for 5 minutes. The supernatant was once more discarded. The B lymphocytes were resuspended in 0.5% Tween/PBS at room temperature and analyzed by the Gallios flow cytometer (Beckman Coulter).

11.8.1 Flow cytometry analysis using Kaluza (Beckman Coulter)

Initially, the flow cytometry panel had to be optimized using single-stained cells with one antibody only, one negative control containing unstained cells, and one containing the EBER probe. The negative control tube was to ensure there was no background fluorescence. Following this procedure, optimal voltage and compensations could be established, as shown in Table 11.3. Compensation was required to correct for overlapping emission spectra of antibodies.

The results of this optimization gave flow cytometer voltages, as shown in Table 15.2 and compensations used are in Table 11.3. Kaluza software (Beckman Coulter) was used to visualize event count and scatter as well as allow compensation and voltage adjustments. The compensations used for the flow cytometry analysis were determined by using single stains of antibodies and probe and the Y-axis median value, which must be equal between positive and negative cell populations. The subsequent compensation values for both healthy control samples and LCLs are shown in Table 11.3 and Table 11.4, respectively.

Laser Channels	FL1 (FITC)	FL2 (PE)	FL3 (PE-CF594)	FL5 (Pe-Cy7)	FL8 (APC-H7)	FL9 (BV421)	FL10 (BV510)
FL1 (FITC)		0	0	0	0	0	0
FL2 (PE)	30.60		6.90	0	0	0	0
FL3 (PE-CF594)	29.00	20.20		0	0	0	0
FL5 (Pe-Cy7)	55.00	0	21.18		0	0	0
FL8 (APC-H7)	2.83	0	0	0		0	0
FL9 (BV421)	57.64	0	0	0	0		8.87
FL10 (BV510)	80.79	4.93	0	0	0	3.94	

Table 11.3 Healthy control compensations used for each laser channel with fluorophores. Compensations were adjusted in Kaluza for flow cytometry analysis of healthy control samples to allow accurate quantification of stained cells.

Laser Channels	FL1 (FITC)	FL2 (PE)	FL3 (PE-CF594)	FL5 (Pe-Cy7)	FL8 (APC-H7)	FL9 (BV421)	FL10 (BV510)
FL1 (FITC)		14.78	21.54	2.00	0.75	1.30	0.00
FL2 (PE)	28.08		52.75	2.00	2.50	0.99	0.00
FL3 (PE-CF594)	5.42	20.20		7.00	2.95	0.99	0.00
FL5 (Pe-Cy7)	0.00	0.00	16.00		5.90	0.20	0.00
FL8 (APC-H7)	0.00	0.00	13.41	9.50		0.00	0.00
FL9 (BV421)	0.00	0.00	21.60	4.00	2.50		15.27
FL10 (BV510)	2.48	4.93	21.75	2.50	0.12	2.50	

Table 11.4 Lymphoblastoid cell line (LCL) compensations used for each laser channel with fluorophores. Compensations were adjusted in Kaluza for flow cytometry analysis of LCL to allow accurate quantification of stained cells.

11.8.2 Gating strategy for B lymphocyte subsets and EBER probe

As shown in Figure 11.1, B lymphocyte subsets and EBER probe were distinguished by gating of the light scatter profiles from the cell populations tested by flow cytometry. The events detected by the flow cytometer were counted over time and these were gated as “Events” as shown in Figure 11.1(a). The start and end of the sample detection were not included to avoid cell debris. The forward and side scatterplot was gated on these “Events” and the cell population shown in Figure 11.1(b) was gated for lymphocyte populations to avoid non-lymphocytes. The forward scatterplot in Figure 11.1(c) compared the width of the cells with the area of the cells and enabled separation of doubled-up cells for single cells, or “singlets”, when gated against the lymphocytes

population in Figure 11.1(b). The positive EBER events, shown as “EBER Positive” in Figure 11.1(d), were gated for by a histogram count of singlet events in the FITC channel when compared to a negative EBER population. These EBER positive events were gated on by subsequent B cell subset scatterplots, as shown in Figure 11.1(e-i). Plasmablasts, which are C19+/CD20-, were gated by the lower right quadrant of the scatterplot between channels for CD20/APC-H7 and CD19/PE. In the scatterplot for channels CD27/BV510 and IgD/Pe-Cy7, switched memory B lymphocytes (CD27+/IgD-), non-switched memory B lymphocytes (CD27+/IgD+), and naïve B lymphocytes (CD27-/IgD+) were gated by the upper left, upper right, and lower right quadrants, respectively. Immature transitional B lymphocytes (CD38++/CD24++) were gated by the far upper right quadrant of the scatterplot for channels CD24/Pe-Cy7 and CD38/BV421. Mature memory B lymphocytes (CD27+/CD19+) were gated by the upper right quadrant of the scatterplot for channels CD19/PE and CD27/BV510.

Figure 11.1. Gating strategy for B lymphocyte subsets. a) Initially, the histogram plot of flow events is gated to exclude the initial and final events from analysis and these are gated upon in b) in a scatterplot of forward scatter and side scatter where the lymphocyte population is gated, and the cell debris is excluded. c) Doublet cells were discriminated against by gating the lymphocytes in a forward scatterplot of cell width vs cell area. These ‘singlets’ are gated on by d) histogram plot of EBER/FITC events, with EBER positive

events gated on by the remaining B lymphocyte subset gates. e) CD38++/CD27++ EBER positive events were gated for by scatterplot of fluorophores BV510 and BV421. f) CD27+/CD20- EBER positive plasmablasts were gated for by scatterplot of fluorophores PE and APC-H7. g) EBER positive class-switched memory B lymphocytes (CD27+/IgD-), non-class switched memory B lymphocytes (CD27+/IgD+) and naïve B lymphocytes (CD27-/IgD+) were gated for by scatterplot of fluorophores BV510 and Pe-Cy7. h) EBER positive immature transitional B lymphocytes (CD24++/CD38++) were gated for by scatterplot of fluorophores of PE-Cf594 and BV421 and i) EBER positive mature memory B lymphocytes (CD19+/CD27+) were gated for by scatterplot of fluorophores of PE and BV510.

12 Results

12.1 RNA extraction results (Nanodrop and gel electrophoresis)

After RNA extraction, the product was measured using Nanodrop spectrophotometry. The mean RNA concentration of 38 samples was 31.02 ng/mL, ranging from 8.3 ng/mL to 87.76 ng/mL.

For additional confirmation of product, purity and state of degradation, extracted RNA was also visualised after 1% agarose gel electrophoresis and compared to a 1Kbp Plus DNA molecular weight ladder. The RNA displayed fragments of multiple lengths ranging from 500bp to 2000bp, as observed in Figure 12.1. Of note, only two RNA samples are presented here. As spectral absorbance of DNA and RNA samples is different, the ratio of absorbance at 260nm and 280nm was determined. Nanodrop spectrophotometry determined and resulted in a mean ratio of 1.70 in samples, ranging from 1.36 to 2.13.

Figure 12.1. RNA extraction products from two healthy controls in 1% agarose gel. Lane 1 and 2 are healthy control RNA with multiple fragments at varying lengths between 500bp and 1000bp.

12.2 HLA-C PCR results

HLA-C PCR was performed to test if RNA extracted samples still contained partial genomic DNA. The agarose gel electrophoresis of the HLA-C PCR products exhibited bands of expected band lengths for RNA and DNA of 1Kbp and 3kbp respectively for most samples (Figure 12.2). Of note, only 20 of the 38 samples were visually tested. The correct RNA fragment was visible in all samples except for Sample 1 and was absent in the negative controls. Similarly, DNA bands were present in all samples, but not the negative controls and Sample 1, despite performing DNAse treatment on extracted samples twice. In addition to the DNA fragment of 3Kbp, samples contained shorter fragments. While bands were absent in all negative controls, band intensity varied considerably between samples.

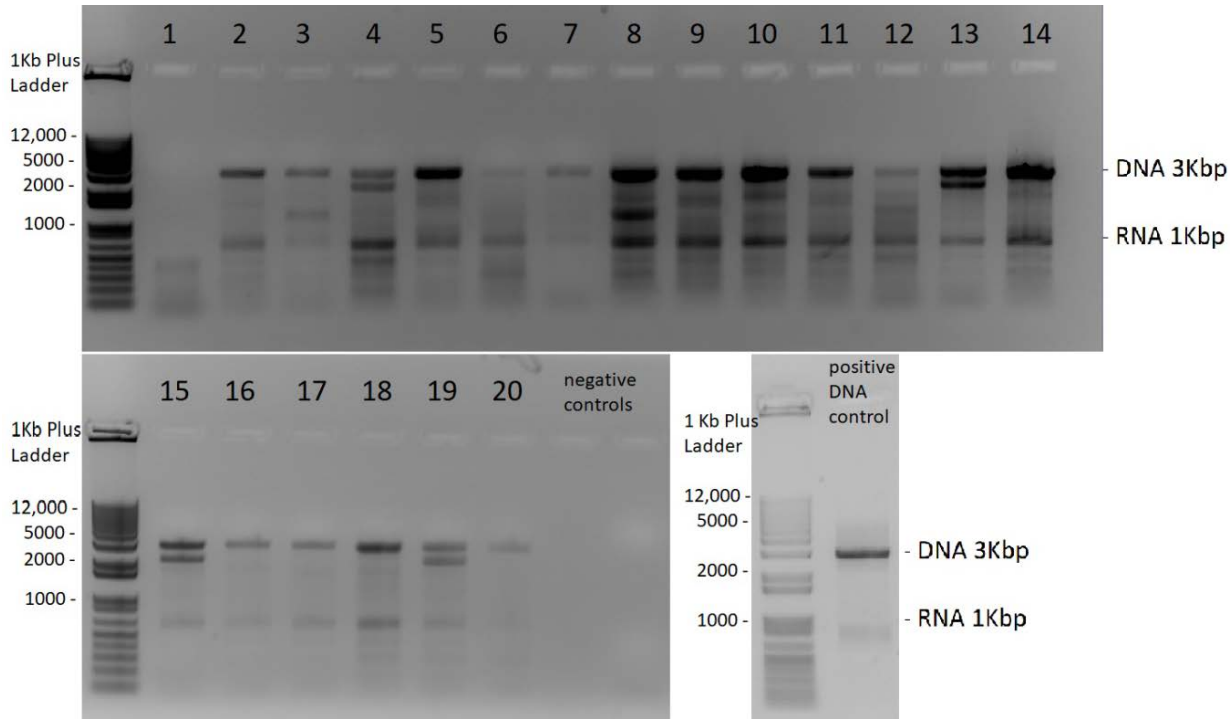

Figure 12.2. Results of HLA-C PCR gel electrophoresis on a 1% agarose gel. Lanes 1 to 20 represent healthy control samples. 1Kbp fragments represent the successful RNA, 3Kbp represent genomic DNA amplification. Of note, additional shorter bands were visible in all samples except for the negative controls.

12.3 Quantification of EBNA-1 by digital droplet PCR (ddPCR)

12.3.1 Optimisation of ddPCR

EvaGreen ddPCR uses a fluorescent dye specific for amplified DNA and oil that separates DNA, resulting in one copy of DNA in each oil droplet. Importantly, this assay detects the presence of any type of amplified DNA and is therefore reliant on the specificity of the EBNA-1 primers to ensure only the target EBNA-1 DNA was amplified.

Dilutions of 1:100, 1:1000 and 1:10,000 of the lymphoblastoid cell line Daudi were used as a positive control. The 1:1000 and 1:10,000 dilutions were successfully quantified by the ddPCR reader with 1428 copies/mL and 282 copies/mL, respectively. The more concentrated Daudi dilution of 1:100 did not lie within the measuring range of the machine and was out of range at the upper end. ddPCR products were additionally visualised by agarose gel electrophoresis to test for amplicon length and therefore primer specificity. As observed in Figure 12.3, the expected fragment of 850bp was clearly visible in all three dilutions of the positive control. However, additional fragments of shorter length were also present (~100bp, ~250bp, ~380bp). In the next step, the smaller DNA fragments were purified separately from the agarose gel and sequenced to test if they represent EBV or unspecific genomic DNA amplification. Sequencing results with the two EBV specific primers did not result in a positive signal.

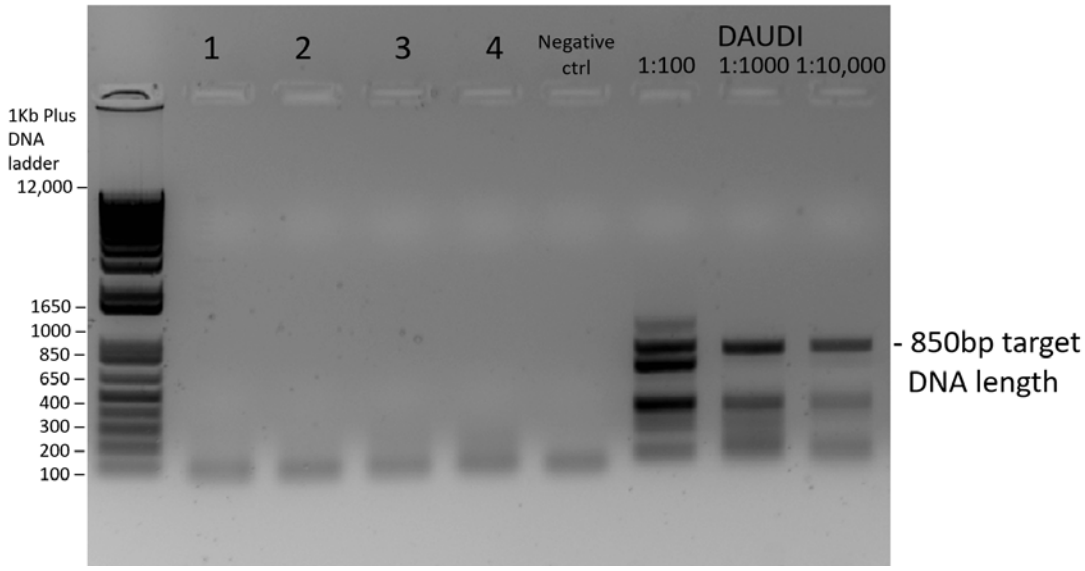

Figure 12.3. Post-ddPCR amplicons of two healthy controls, two LCLs and three positive control Daudi dilutions from 1:100 to 1:10,000 on a 1% agarose gel. Lanes 1 and 2 are healthy controls and lanes 3 and 4 are LCLs. None of these samples were amplified, as the only bands present are from primer dimers. The target fragment length of this PCR was 850bp, however, amplicons at multiple lengths, including 850bp, were visualised for the Daudi dilutions. These non-target fragments were present at lengths ~100bp, ~250bp and ~380bp at decreasing intensity with decreasing dilution.

The primers used in this method were previously developed by Dr. Monika Tschochner for use in nested PCR for amplification of part of the EBNA-1 gene from DNA templates (69). The high homology of EBNA-1 to genomic DNA has previously been reported in many studies (8–10). Therefore, to reduce non-specific amplification due to EBNA-1 homology with genomic DNA, as shown in the Daudi results, it was speculated that this could be reduced by starting with an RNA template rather than a DNA template.

In the first experiment, two healthy control samples and two LCL samples were tested and analysed by ddPCR. Of the two healthy control samples tested, neither were detected and no fragments post-amplification were visualised on a 1% agarose gel (Figure 12.3). One of the two LCL samples were quantified by the ddPCR reader in parallel to the

healthy controls, and were measured to contain 2158 DNA copies/mL detected. However, this LCL sample did not present any fragments when visualised by agarose gel electrophoresis. It was later determined that the ddPCR oil used was expired as confirmed by laboratory technicians. However, this method was not repeated with fresh ddPCR oil and healthy controls samples as the sequencing results of the Daudi positive control fragments confirmed the ddPCR reader to be quantifying non-EBNA-1 DNA. As a result, this method was not tested on further samples due to amplification of multiple non-specific fragments.

12.4 Quantification of EBNA-1 by quantitative PCR (qPCR)

12.4.1 qPCR standard development

A standard of known EBNA-1 DNA copies was required to calculate EBV copies of unknown samples. To obtain a standard for qPCR, a purified EBV plasmid was used that spanned positions 389bp to 641bp of EBNA-1. A PCR was performed to amplify part of the EBV plasmid and sequenced. This sequence was confirmed to match N terminal EBNA-1 and is given in Table 12.1. The amplified PCR product EBNA-1 was measured using spectrophotometry (Nanodrop) in triplicate, with results 38.07 ng/µL, 43.52 ng/µL and 25.81 ng/µL. The mean concentration of the EBNA-1 standard stock solution was 35.8 ng/µL with a standard deviation of 9.07. The DNA copy number in the standard was determined using the following formula:

$$\textit{Number of DNA copies} = [\textit{amount of amplicon(ng)} \times 6.0221 \times 10^{23} \textit{molecules/mole}]$$

$$/[\textit{length of DNA amplicon} \times 660 \textit{ng/mole} \times 1 \times 10^{9} \textit{ng/g}]$$

Using the mean Nanodrop measurement as the basis, the mean number of DNA copies for the stock standard solution was calculated to be 6.84×10^{11} copies of EBNA-1 DNA.

To allow for measurement in the linear range of the qPCR machine, the standard was 1:10 serially diluted as depicted in Table 12.2. This standard was used in all subsequent qPCR experiments to calculate EBV copy numbers of unknown samples.

3'CACAATGTCGTCTTACACCATTGAGTCGTCTCCCCTTTGGAATGGCCCCT
GGACCCGGCCCACAACCTGGCCCGCTAAGGGAGTCCATTGTCTGTT5'

Table 12.1. Sequence of qPCR amplified 97bp EBNA-1 fragment from position 389 to 641 as sequenced by Next Generation Sequencing.

To optimise the concentrations of qPCR primers and probe used (QIAGEN, US), the standard was tested by qPCR initially at 350nM of forward and reverse primer and 180nM of the probe, as recommended by the manufacturer. However, it was confirmed that primer dimers were seen when the amplicons were visualised on a 3% agarose gel, hence the concentrations of the primers and probe were reduced to 200nM and 170nM, respectively.

The standard was tested in qPCR and Cq values were determined as demonstrated in Table 12.2. As it was unknown which DNA concentrations were detectable by qPCR, six dilutions of the standard were initially tested. Five out of the six dilutions of the standard were detected by qPCR, however, only three dilutions (684,000, 68,400 and 6840 DNA copies) were successfully replicated. Hence, these three dilutions were used for standard curve analysis. Performance of the standard was analysed by standard deviation, variance, and coefficient of determination, as given in Table 12.2, and the standard was determined to be highly reproducible. The limit of detection of the standard was calculated as 6.84 copies of EBNA-1 DNA (see 11.6.3 for qPCR calculations). However, it could not be consistently detected at this low level every time. The limit of quantification, or the lowest concentration of the standard detected consistently in every assay, was 6840 copies of EBNA-1 DNA.

DNA copies	$\log_{10}$[DNA copies]	Mean Cq	Median	Standard deviation	Variance	R^2
684000	5.84	29.65	29.60	1.02	1.03	0.98
68400	4.84	32.82	32.8	0.20	0.04	
6840	3.84	36.98	36.97	1.03	1.05	
684	2.84	47.49	47.49	N/A	N/A	
68.4	1.84	Undetected	N/A	N/A	N/A	
6.84	0.835	48.55	48.55	N/A	N/A	

Table 12.2. Comparison of EBNA-1 standard performance between all qPCR assays. Six serial dilutions of the standard were used. The number of amplification cycles, or Cq value, was given at each serial dilution of the standard. The standard deviation and variance were calculated for Cq values that were detected more than twice. The qPCR reader did not detect the standard at concentrations of 684 DNA copy number and 6.84 DNA copy number more than once, and at 68.4 DNA copy number, the standard was not detected at all, as denoted by "undetected" in the table. N/A denoted calculations that could not apply to dilutions as they were not able to be detected more than once.

The qPCR amplification curve in Figure 12.4 represents serial dilutions of the standard by a factor of 10. At less than 68.4 DNA copies of EBNA-1, the amplification curve did not reach the threshold and hence no Cq value could be determined. The threshold was set by the qPCR reader was 100 relative fluorescence units (RFU), however at this threshold initial background "noise" was detected in PCR amplification. Hence, the threshold was raised to 455 RFU, which was above the initial non-specific detection but

less than the lowest standard dilution detected at 6.84 DNA copies. To keep the assay consistent, this threshold was used in each qPCR analysis for all samples.

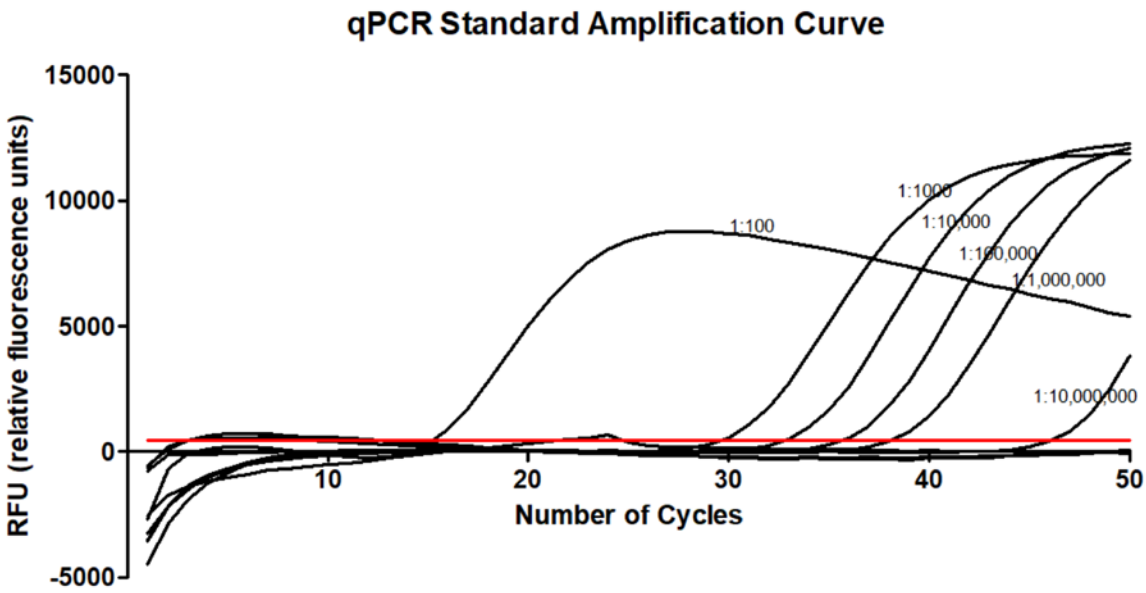

Figure 12.4. Standard qPCR amplification curve with relative fluorescence units (RFU) plotted against the number of cycles with the threshold in red at 455 RFU. Serial dilutions of the standard are demonstrated to $1:10^7$ (equivalent to 68.4 DNA copies).

Amplified healthy control and standard qPCR products were examined by agarose gel electrophoresis to determine the specificity of the primers and probe. The qPCR assay of the standard only amplified the 97bp target, as demonstrated on the agarose gel in Figure 12.5. Three healthy control samples were also tested alongside the standard in this experiment, however, none of these samples were detected by the qPCR reader. An amplified fragment length from the qPCR of healthy control sample 3 was observed on the gel Figure 12.5 at 150bp. However, this was not the target 97bp amplicon for this assay, as advised by the manufacturer.

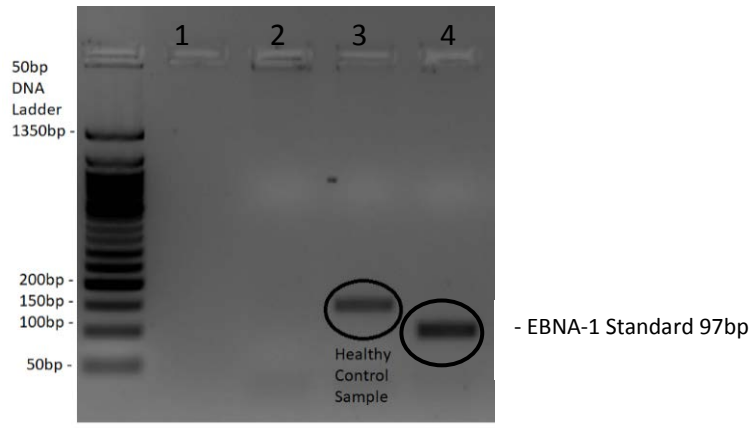

Figure 12.5. qPCR amplified healthy control samples and standard in 3% agarose gel with a 50bp molecular weight DNA ladder. Lanes 1-3 were healthy control samples and Lane 4 was the EBNA-1 qPCR standard (97bp). An amplicon was seen in lane 3 (150bp) with no amplicons detected in lane 1 and lane 2.

The standard curve for the four qPCR assays, as depicted for comparison in Figure.12.6, were analysed for variance. The variance of the Cq values was on average 0.76 cycles between all qPCR standard assays, and the mean standard deviation was 0.75 cycles.

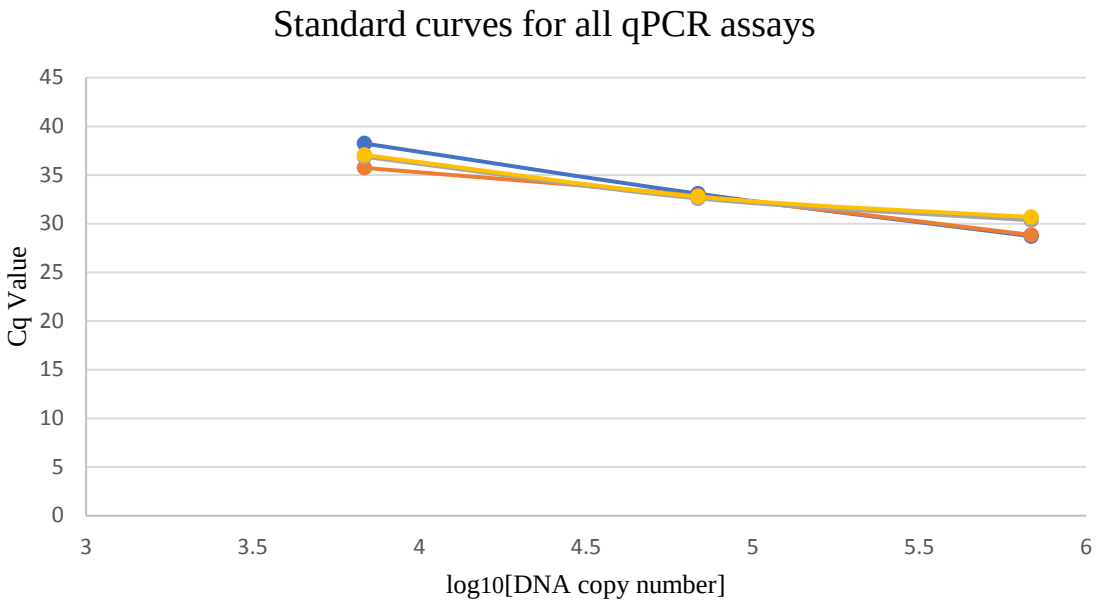

Figure.12.6. Standard curves for all qPCR assays for DNA copy numbers between 6840 copies and 68,400 copies. The standard was detected twice at lower DNA copies however, this was not reproducible.

12.4.2 qPCR analysis of healthy control samples

Out of 38 healthy control samples, 31 samples were successfully quantified by qPCR. All samples were tested in triplicate, however, only fourteen samples were detected in duplicate and three samples were detected in triplicate. Stochastic variation was observed in the assay and only one sample was reproducible in triplicate.

The QIAGEN EBV analyte-specific reagent qPCR kit limit of detection was not established previously by the manufacturer, however, the limit of detection of EBNA-1 in healthy control samples in this experiment was 5 DNA copies/2µL, or 2515 DNA copies/mL (Table 12.3). The limit of quantification was defined as the lowest DNA copy number that could be successfully detected in duplicate. This was 52 DNA copies/2µL, or 26,000 DNA copies/mL for the healthy control samples in this experiment. The mean was 2.18×10^9 DNA copies/100,000 PBMCs and the median was 7.34×10^5 DNA copies/100,000 PBMCs.

Due to the difference in cell count for each sample used, the EBNA-1 DNA copy number was calculated per 100,000 PBMCs to enable accurate comparison between sample results, as tabulated in Table 12.3. The median copy number of EBNA-1 in healthy controls was 7.34×10^5 DNA copies/100,000 PBMCs. The range between EBNA-1 DNA copy numbers was between 23 DNA copies/100,000 PBMCs and 4.34×10^{10} DNA copies/100,000 PBMCs. The mean was 2.18×10^9 DNA copies/100,000 PBMCs. The mean EBNA-1 DNA copy numbers for the 38 healthy control samples tested were also presented in a logarithmic form for sample comparison in Figure 12.7.

Sample	qPCR Test 1	qPCR Test 2	qPCR Test 3	Mean	Standard Deviation	Mean DNA copies/100,000 PBMCs
1	-	-	-	-	-	-
2	2.26×10^4	5113.09	-	1.39×10^4	-	1.19×10^4
3	68.17	3.11×10^4	-	1.56×10^4	-	35.87
4	-	-	-	-	-	-
5	3947.13	1.08×10^7	-	5.41×10^6	-	1.44×10^7
6	100.15	-	-	-	-	4.34×10^{10}
7	3.16×10^6	-	-	-	-	1.13×10^5
8	4.78×10^{12}	2.65×10^9	-	2.39×10^{12}	-	7.96×10^{12}
9	9018.17	5.69×10^6	-	2.85×10^6	-	1.31×10^6
10	3.11×10^4	-	-	-	-	1.11×10^8
11	7577.41	1.04×10^5	465.88	3.74×10^4	5.79×10^4	1.46×10^4
12	-	-	-	-	-	-
13	7212.55	15.06	-	3613.80	-	2.03×10^9
14	1.08×10^9	-	-	-	-	9.82×10^8
15	3492.96	5.01×10^5	1.01×10^4	1.72×10^5	2.85×10^5	8.59×10^4
16	-	-	-	-	-	-
17	1692.73	-	-	-	-	4.38×10^7
18	3.76×10^8	-	-	-	-	5.57×10^8
19	52.44	51.72	-	52.08	-	76.59
20	6.77×10^7	-	-	-	-	6.45×10^7
21	5.65×10^5	-	-	-	-	3.890×10^5
22	8247.69	-	-	-	-	1.38×10^4
23	1.13×10^9	2825.40	1.65×10^9	3.76×10^8	6.52×10^8	2.26×10^8
24	-	-	-	-	-	-
25	51.99	3408.20	-	1730.10	-	1038.06
26	1.60×10^6	-	-	-	-	1040.38
27	-	-	-	-	-	-
28	4.18×10^6	43.67	-	2.09×10^6	-	1.72×10^5
29	35.77	1.17×10^4	-	5871.32	-	396.36
30	78.75	9.96×10^{10}	-	497×10^{10}	-	7.58×10^9
31	1646.07	-	-	-	-	44.49
32	1.18×10^6	28.13	-	5.90×10^5	-	4.21×10^4
33	2.06×10^8	-	-	-	-	1.65×10^9
34	5.03	-	-	-	-	0.38
35	-	-	-	-	-	-
36	16.97	-	-	-	-	23.15
37	-	-	-	-	-	-
38	5.74×10^5	516.92	-	2.87×10^5	-	1.08×10^6

Table 12.3. EBNA-1 DNA copy numbers of healthy control samples were tested in triplicate with qPCR and results are given per 100,000 PBMCs. Yellow shaded samples were successfully detected in duplicate and grey shaded samples were successfully detected in triplicate. The standard deviation was only given for samples detected in triplicate. Samples not detected are denoted by "-".

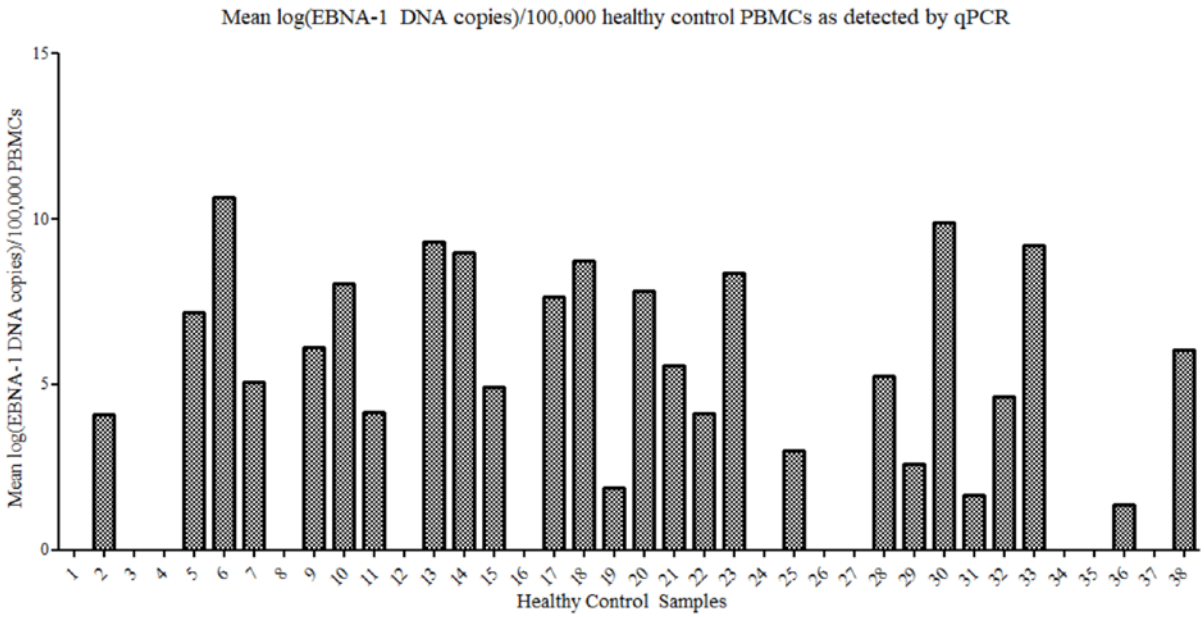

Figure 12.7. Mean number of log[EBNA-1 DNA copies] per 100,000 PBMCs quantified by qPCR in 38 healthy control patient samples. The range of healthy control samples was between log[1.36 DNA copies]/100,000 PBMCs (or 23 DNA copies/100,000 PBMCs) and log[10.64 DNA copies]/100,000 PBMCs (or 4.34 x 10^{10} DNA copies/100,000 PBMCs). Samples 1, 3, 4, 8, 12, 16, 24, 26, 27, 34 and 35 were not detected by qPCR. Note that the sample identification numbers are arbitrary in relation to other graphical analysis of samples provided in this study.

12.4.3 qPCR performance

After amplification by qPCR, the healthy control sample amplicons were tested for specificity by visualisation on a 3% agarose gel, as demonstrated in Figure 12.8. The gel results enabled comparison between the qPCR results and the amplified fragment length to test the specificity of the probe with healthy control samples. The target fragment length of 97bp was visualised on agarose gel for healthy control samples that also were successfully detected by qPCR. Samples not detected by qPCR, but appeared on the agarose gel image, were not 97bp fragments. However, some samples were detected by qPCR at copy numbers >1000 DNA copies but did not appear on an agarose gel.

The serially diluted standard tested alongside healthy control samples was also visualised on an agarose gel (Figure 12.8) after qPCR amplification to confirm probe specificity. The fragments were presented at length 97bp between 1:10,000 dilution (6.84×10^7 DNA copies) and 1:10billion (68.4 DNA copies). When the dilution was $>6.84 \times 10^7$ DNA copies, a smear was visualised due to the very high concentration of products present. At these concentrations, the standard was detected by qPCR. At less than 68.4 copies of DNA, the standard was unreliably detected by the qPCR machine and on an agarose gel depicted in Figure 12.8, the fragments were not visible when less than 68.4 copies of DNA were present. This supported the limit of detection by the qPCR machine. In the absence of a 97bp band on the agarose gel or the presence of bands at higher or lower lengths, the sample was not detected by qPCR.

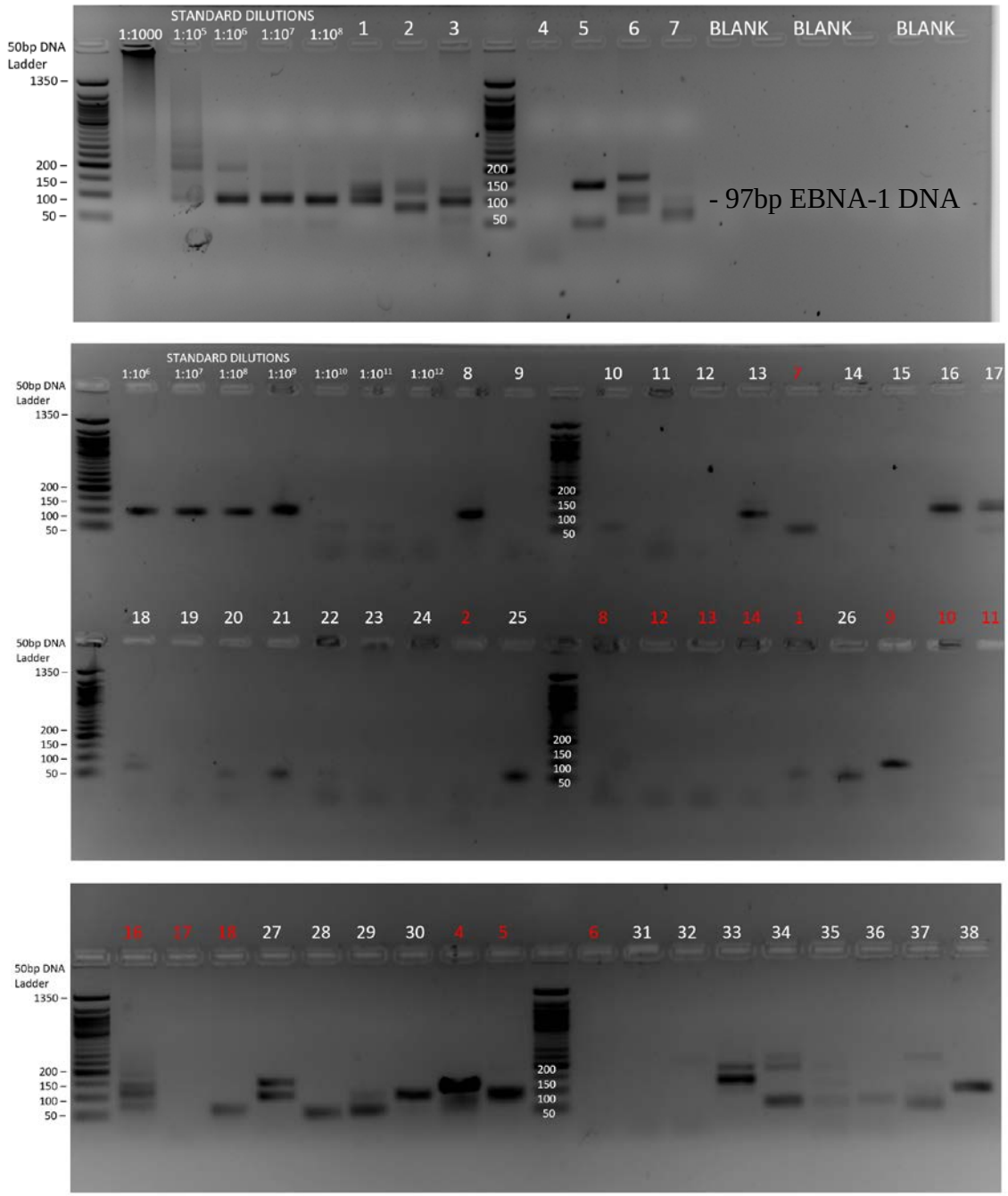

Figure 12.8. qPCR amplicons displayed on 3% agarose gels. Results of two separate qPCR experiments are shown including assay standards in 10-fold dilutions. Standard dilutions below 1:10billion, equivalent to 68 copies of EBNA-1 DNA, were negative. The healthy control samples numbered in red represent duplicate samples. Samples 1, 3, 6, 8, 13, 16, 17, 26, 27, 30, 34 and 37 all demonstrated strong bands at the expected fragment length of 97bp. Note: the numbers of the samples in this figure do not correspond to the numbers allocated to samples in other figures/tables.

The average amplification efficiency of this qPCR assay was determined to be 95.75% with a 3.49 amplification cycle (Cq value) change between standard dilutions, as derived from the mean slope of the standard curve. This calculation was derived from Bio-Rad (126) and as displayed in Figure.16.4, the threshold cycle was plotted against the $\log_{10}$[DNA copy number] of the standard with a regression line.

12.5 Quantification of EBER by flow cytometry coupled with fluorescent in situ hybridisation (Flow-FISH)

12.5.1 B lymphocyte enrichment results

The isolation of B lymphocytes by negative selection from two healthy control PBMC samples yielded high retention of B lymphocyte-enriched populations. B lymphocyte s are a minor population of PBMCs, hence >50million PBMCs were thawed for each sample. The comparative cell count between pre-B lymphocyte isolation and post-B lymphocyte isolations for each sample are listed in Table 12.4. The viability of the cells was very high (98%) and the percentage of B lymphocytes from PBMCs for samples 1 and 2 was 8.46% and 19.33%, respectively.

Sample	Pre-B cell Isolation count	Post-B cell Isolation count	Viability	B Cell % of PBMCs
1	55 x 10^6 cells	4.65 x 10^6 cells	98%	8.46%
2	60 x 10^6 cells	11.6 x 10^6 cells	98%	19.33%

Table 12.4 B lymphocyte enrichment for downstream flow cytometry analysis. Viability was high and B lymphocyte counts were 4.65 x 10^6 and 11.6 x 10^6 cells respectively for the two samples.

12.5.2 LCL flow-FISH results

The LCLs were used as a positive control for EBER flow-FISH as they are EBV-transformed cells and hence were expected to harbour EBV in all B lymphocyte clones. As expected, EBER RNA was successfully detected in duplicate in LCLs. The initial testing of LCLs with flow-FISH resulted in 8380 EBER positive events out of 111,360 LCLs, which was equivalent to 4.46%. While, not all LCLs were EBV positive, the histogram counts and scatterplot of these EBER events confirms a clear positive shift to the right, measured by flow cytometry as portrayed in Figure 12.9 (a and c). A similar result was demonstrated when this was repeated with the same sample, resulting in 5549 positive EBER events in 62,385 LCLs, which was equivalent to 5.55% positive EBER events. Again, Figure 12.9 (b and d), the EBER events demonstrated a positive shift of events to the right.

Figure 12.9. LCL EBER probe Kaluza flow cytometry analysis. The initial testing of LCLs with the EBER probe resulted in 4.46% positive EBER events in 111,360 LCLs, as illustrated in a) a histogram plot of EBER events as detected by the FITC fluorophore channel and b) a scatterplot of side light scatter and EBER with a positive population shifted to the right in both the histogram and scatterplot. Similar results were seen when the assay was repeated with the same LCL sample (b and d) with 5.55% positive events in 62,385 LCLs.

As LCLs are transformed cells, the cell properties are often different to isolated B lymphocytes. Hence, it was necessary for the voltages and compensations established for the LCL sample to be different from the B lymphocyte samples. The presence of surface markers on LCLs was determined. Interestingly, only anti-CD20 and anti-CD38 antibodies bound the LCLs at 5.95% and 2.65% of events respectively, as depicted in Figure 12.10.d-e. The remaining antibodies were not detected by flow cytometry in the LCL sample, as illustrated in Figure 12.10.a-c, f.

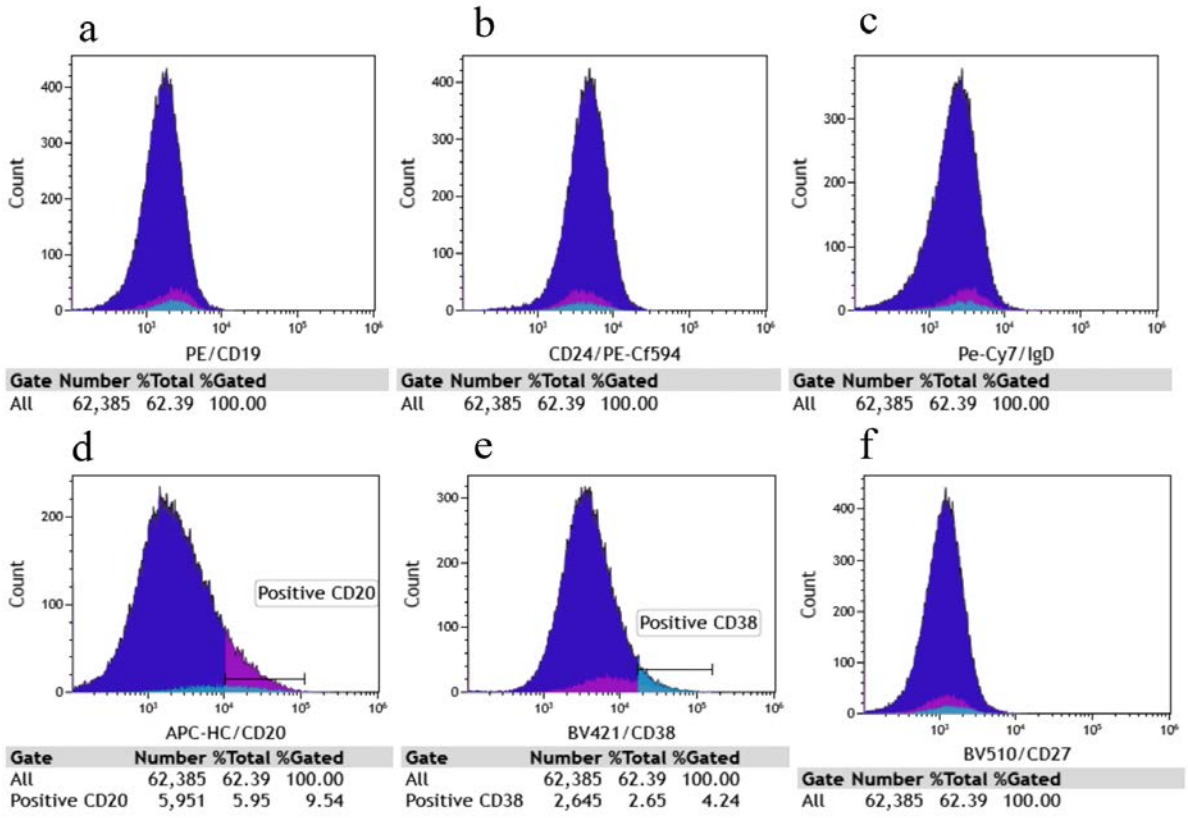

Figure 12.10. LCL stained with all antibodies event counts as detected by flow cytometry and analysed by Kaluza. CD19, CD24, IgD and CD27 populations were not detected as depicted in event histogram a), b), c) and f). Histograms d) and e) demonstrate positive CD20 and CD38 populations, respectively, by the clear shift to the right. CD20 was detected in 5.95% of LCLs and CD38 was detected in 2.65% of LCLs. The dark purple represents all events and the blue and magenta shading represent the proportions of positive CD38 and positive CD20 cells, respectively.

12.5.3 B lymphocyte phenotyping results

The antibodies for the B lymphocyte surface markers were tested in single stains by flow cytometry analysis in two healthy control PBMC populations to determine surface marker expression in B lymphocytes. As summarised in Table 12.4, in the presence of the EBER probe, Sample and 1 and 2 had positive events for all antibodies except CD19, which had very low binding efficiency. This resulted in difficulty determining positive populations for CD19. This was contradicted when the single stain sample for CD19 in the absence of the EBER probe was overlayed on the CD19-negative sample with a positive population observed (Figure 12.11.a). All positive antibody stains were compared to the negative sample and the negative and positive population plots overlayed, as seen in Figure 12.11.b-e. The overlay of the positive single stain population for each antibody on the negative population demonstrated a clear distinction of positive events.

Mean percentage of cells measured by flow-cytometer for samples in the presence of EBER probe						
Healthy Control	CD19	CD20	CD24	IgD	CD27	CD38
Sample 1 PBMCs	0.79%	5.01%	4.75%	4.02%	15.18%	13.24%
Sample 1 B cells	0.10%	37.13%	0.39%	32.10%	0.65%	38.37%
Sample 2 PBMCs	3.41%	7.17%	4.87%	5.49%	50.92%	47.45%
Sample 2 B cells	0.24%	55.75%	0.40%	23.39%	4.03%	43.24%

Table 12.5. Mean percentage of surface marker events in the presence of EBER probe as measured by Gallios flow-cytometer comparing PBMC populations and B lymphocyte - enriched populations from the same healthy control patients.

In B lymphocyte enriched populations, the antibodies anti-CD20/APC-HC and anti-IgD/Pe-Cy7 had high binding efficiency, as depicted in Table 12.5. Anti-CD19/PE had low binding efficiency for both populations, as demonstrated by the low mean percentage of events in Table 12.5. Anti-CD24/PE-Cf594, anti-CD27/BV510, and anti-CD38/BV421 had inconsistent binding efficiency in the presence of the EBER probe as the number of events decreased instead of increasing when the population was B lymphocyte enriched.

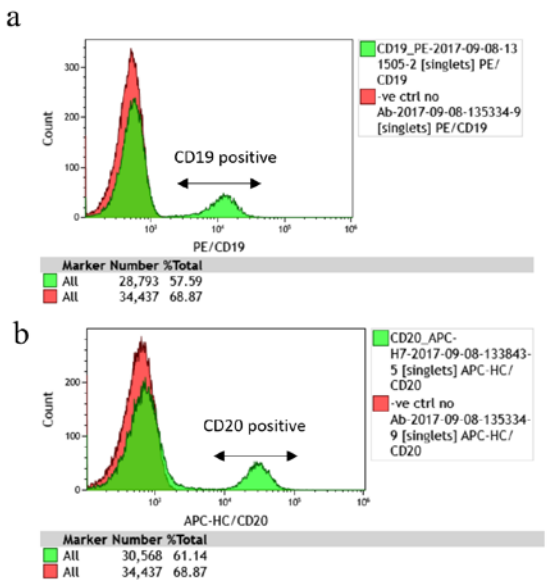

Figure 12.11. Overlays of positive single stain population over unstained PBMC populations in the absence of EBER probe, as measured by Gallios flow-cytometer. The negative populations depicted (in red) were overlayed on the positive populations (in green). Shown from top to bottom are the single staining of a) anti-CD19 antibody labelled with PE, b) anti-CD20 antibody labelled with APC-HC, c) anti-CD24 antibody labelled with PE-CF594, d) anti-CD27 antibody labelled with BV510, e) anti-CD38 antibody labelled with BV421, and f) anti-IgD antibody labelled with Pe-Cy7, all overlayed on negative populations. Whilst overlays a) to c) demonstrate uniform populations, the overlays for d) and e) (CD27 and CD38, respectively) displayed equal negative and positive populations in the positive stains.

12.5.4 B lymphocyte EBER probe results

EBER RNA in B lymphocyte s was successfully detected by flow cytometry in healthy control B lymphocyte -enriched populations and PBMC populations. 4% of the PBMC population from Sample 1 were positive EBER events. 5% of the PBMC population from Sample 2 were positive EBER events. For the initial testing of Sample 1, 1% of enriched B lymphocyte s were EBER positive events, whilst 21% of enriched B lymphocyte s from Sample 2 were EBER positive. However, when this was replicated, 31% and 38% of enriched B lymphocyte s were EBER positive events from Sample 1 and 2 respectively. B lymphocyte enriched samples were tested in duplicate with approximately 1 million enriched B lymphocytes in the first test and 5million B lymphocytes in the second. The EBER probe was detected in cells in both samples by flow cytometry, as demonstrated in Table 12.5. These results were established by histogram overlay of the EBER positive population over the EBER negative population, to compare the positive population shift to the right, as depicted in Figure 12.12.

Percentage of EBER-positive cells measured by Gallios flow-cytometer							
Sample type	All EBER	Immature transitional	Naïve	Memory	Non-switched	Plasmablast	Switched
			Healthy control sample 1				
PBMCs	4%	0.02%	0.91%	0%	1.96%	0.02%	0.44%
B cell (1)	1%	0%	0.86%	0%	0%	0%	0%
B cell (2)	31%	0.06%	15.89%	0.01%	14.17%	0%	0.49%
			Healthy control sample 2				
PBMCs	5%	0.37%	0.11%	0%	3.56%	0%	1.44%
B cell (1)	21%	0.01%	14.31%	0.19%	3.13%	0.04%	1.18%
B cell (2)	38%	0%	34.08%	0.01%	2.75%	0%	0.23%
MEAN	16.67%	0.08%	11.03%	0.04%	4.26%	0.01%	0.63%

Table 12.6. Percentage of EBER-positive cells measured by Gallios flow cytometer. Measured positive EBER events as well as positive antibody surface markers that are gated by the different B lymphocyte subsets transitional B lymphocytes, naïve B lymphocytes, memory B lymphocytes, switched B lymphocytes, non-switched B lymphocytes and plasmablasts. The B lymphocyte healthy control samples were tested twice, as annotated by (1) or (2). For test (1), 1 million B lymphocytes were analysed and for test (2) 5-8million B lymphocytes were analysed.

Figure 12.12. Overlay comparisons between positive and negative EBER populations. Healthy control sample 1 was assessed twice with flow-FISH for positive EBER B lymphocytes and overlayed on the negative population in a) and b). Sample 2 was also assessed twice with flow-FISH and the positive EBER B lymphocytes were overlayed on the negative population in c) and d).

Using the gating strategy described in the methods (11.8.2 Gating strategy for B lymphocyte subsets and EBER probe), the B lymphocyte subsets were gated and the EBER ratio between each subset was determined. As demonstrated in Table 12.6, naïve B lymphocytes were the most positive for EBER at an average of 11.03% of EBER-positive cells with non-switched memory B lymphocytes at an average of 4.26% of EBER-positive cells. Immature transitional B lymphocytes, memory B lymphocytes, plasmablasts and switched memory B lymphocytes had the lowest average detection of EBER events at 0.08%, 0.04%, 0.01% and 0.63%, respectively. These percentages were derived from scatterplots, as depicted in Figure 12.13 and Figure 12.14.

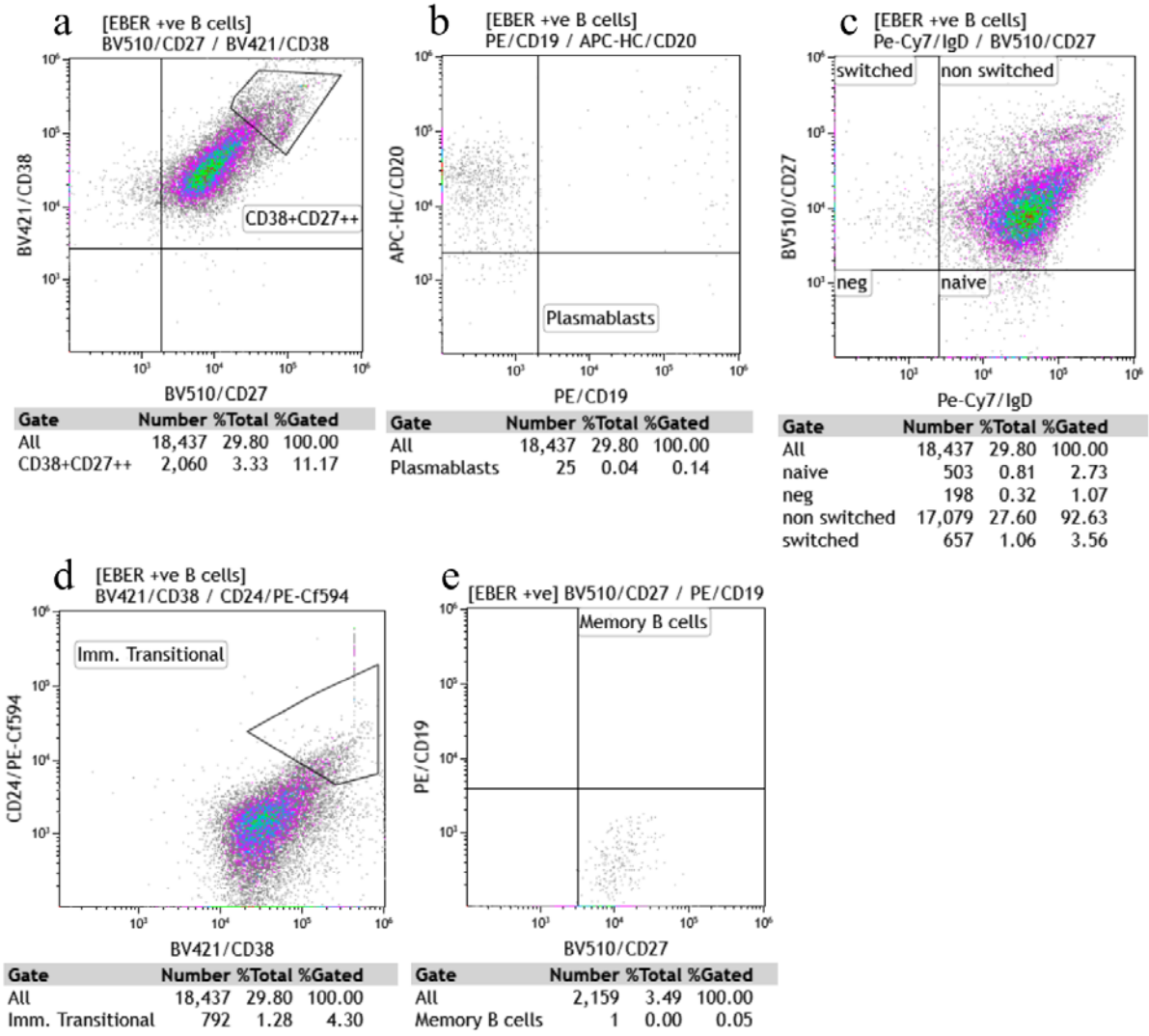

Figure 12.13. Sample 1 B lymphocyte subsets gated on EBER-positive cells. Using the gating strategy described in the methods of this study, B lymphocyte subsets gave percentages of EBER positive plasma lymphocytes, plasma blasts, naïve B lymphocytes, non-class switched memory B lymphocytes, class-switched memory B lymphocytes, immature transitional B lymphocytes and mature memory B lymphocytes out of a total of 18,437 EBER positive B lymphocytes.

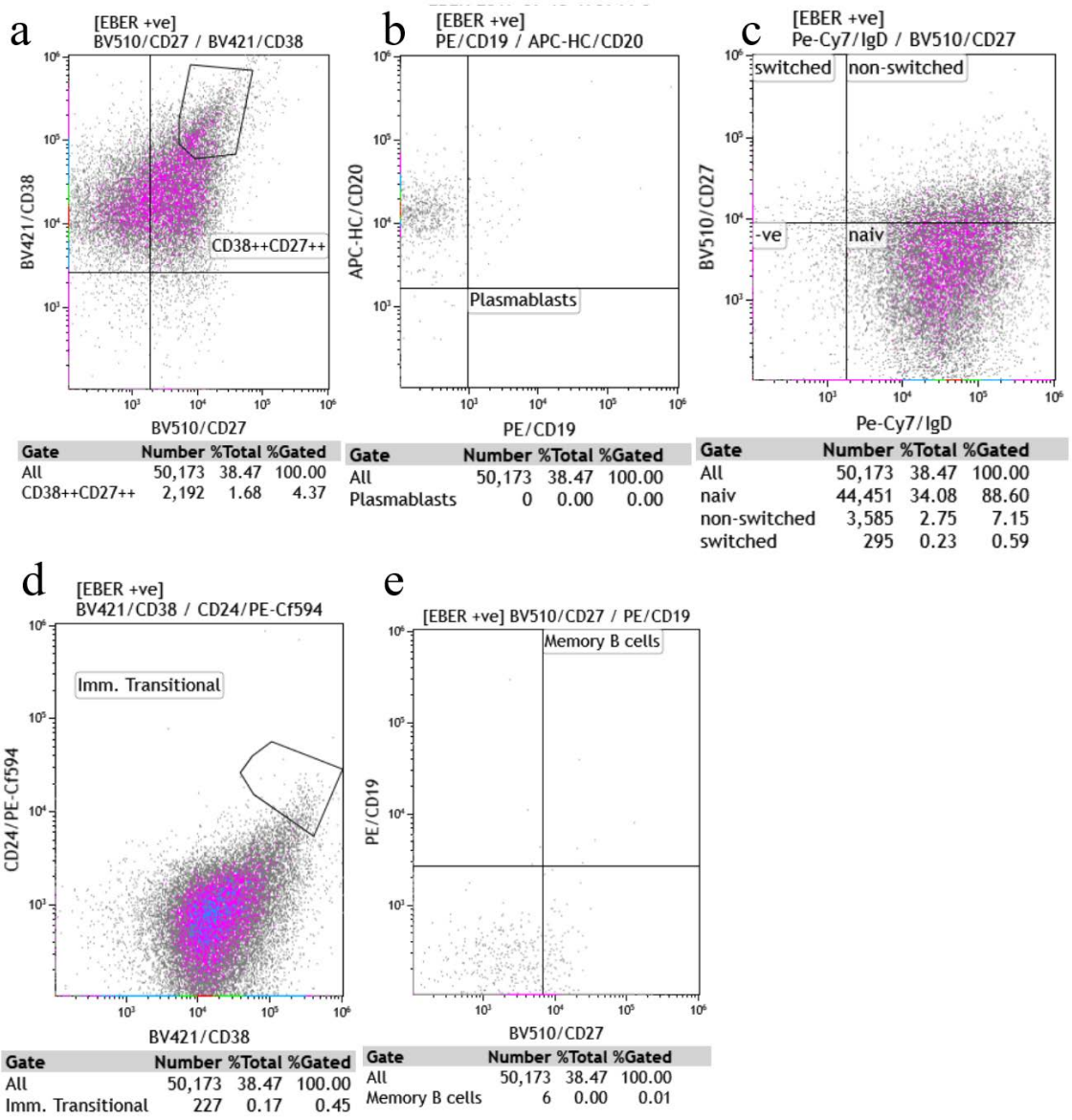

Figure 12.14. Sample 2 B lymphocyte subsets gated on EBER-positive cells. Using the gating strategy described in the methods of this study, B lymphocyte subsets gave percentages of EBER positive plasma lymphocytes, plasma blasts, naïve B lymphocytes, non-class switched memory B lymphocytes, class-switched memory B lymphocytes, immature transitional B lymphocytes and mature memory B lymphocytes out of a total of 50,173 EBER positive B lymphocytes.

12.6 Comparison of EBV quantitative methods

To compare assay performance in detection of EBV, two healthy control samples were tested with all three techniques ddPCR, qPCR and flow-FISH to compare their quantification of EBV. qPCR quantified EBNA-1 in both samples at 1.31 x 10^6 and 1.72 x 10^5 DNA copies/100,000 PBMCs, whilst ddPCR did not detect EBNA-1 in these samples, as presented in Table 12.7. EBER was quantified by flow-FISH for these samples at 4% and 5% EBER-positive cells in 1million PBMCs.

	EBNA-1 DNA copies/100,000 PBMCs		**EBER events/1Mio PBMCs**
Healthy Control Samples	ddPCR	qPCR	Flow-FISH
Sample 1	Not detected	1.31 x 10^6	4%
Sample 2	Not detected	1.72 x 10^5	5%

Table 12.7 Comparison of three quantitative techniques for EBV in two healthy control samples: ddPCR, qPCR and flow-FISH. ddPCR did not detect EBNA-1 in either sample. qPCR and flow-FISH quantified EBNA-1 and EBER in PBMCs.

13 Discussion

It was proposed that three quantitative methods would be compared for the detection of EBV in latency, using EBNA-1 and EBER as targets. Additionally, the ratio of EBV copies in B lymphocyte subsets should be quantified and compared. Healthy control samples were tested for the presence of latent EBV using i) qPCR, ii) ddPCR and iii) flow-FISH. Although only limited number of samples were tested, the quantitative technique ddPCR positive control samples were not quantified and the method was unable to detect EBV in healthy controls in this experiment. In contrast, qPCR and flow-FISH were successful in the detection and quantification of EBNA-1 and EBER, respectively.

Of note, all results were established for healthy control samples only, as ethics approval for MS patient samples was unable to be obtained prior to the completion of this study. All further samples discussed are related to healthy controls only unless stated otherwise.

13.1 Analysis of digital droplet PCR (ddPCR)

13.1.1 Analysis of the use of reverse-transcribed EBNA-1 RNA as a template for quantification

High homology of EBNA-1 with sequences in genomic DNA has been discovered in previous research (69,127). Therefore, for EBV quantification, RNA was reverse-transcribed and utilized as a cDNA template to reduce the likelihood of targeting of genomic DNA non-specifically in downstream assays. A study by Tschochner, et al., has proven that nested PCR can detect EBV in latency in MS patients, but single round PCR amplification from a DNA template was not sensitive or specific enough for EBNA-1 detection (69 and personal communication). Unfortunately, nested PCR was considered to be unsuitable for quantification in ddPCR as only a fraction of the first-round amplicons would serve as a template for nested PCR and the repeated exponential

amplification in two subsequent PCRs would hinder the accurate calculation of DNA copy numbers. Therefore, two-round PCR was deemed unsuitable for the quantification of EBNA-1.

Subsequently, the approach was made to test the sensitivity of ddPCR and to avoid non-specific amplification by utilizing RNA as a template for cDNA conversion, thus avoiding the quantification of genomic DNA homologous to EBNA-1. Furthermore, EBNA-1 is constitutively expressed in infected B cells as the EBV genome is coupled to the host genome for the distribution of daughter cells during mitosis (128). However, as EBNA-1 is also expressed in lytic infection, quantification will occur regardless of the EBV lifecycle stage. The distinction between latent and lytic infection would only be made by comparing absolute copy numbers with an arbitrary delineation between high and low. Alternatively, the addition of a lytic genes involved in viral reactivation from latency and replication, such as BZLF1 or BRLF1, for multiplex PCR would serve as a control in future experiments. In addition, it was proposed the EBNA-1 RNA load would be greater than that of genomic RNA as genomic DNA is not always expressed, unlike EBNA-1, therefore reducing the genomic RNA to EBV RNA ratio when initiating with an RNA template.

Purification of RNA was more challenging than predicted. Despite utilization of a modified RNA extraction method including an additional DNA digestion step with an increased digestion period, DNA was observed when visualised on agarose gel. Additionally, Nanodrop spectrophotometry resulted in an absorbance ratio (mean 1.70) which was less than the expected pure RNA ratio of 2.00.

In parallel, the existence of DNA in the RNA samples was confirmed in HLA-C PCR. Primers of HLA-C are designed to amplify RNA and DNA at different lengths. Significant quantities of DNA were established in the HLA-C PCR agarose gel with

fragments observed at multiple lengths, including the expected length of RNA at 1Kbp and the expected length of DNA at 3Kbp. Of note, multiple additional shorter fragments were amplified in HLA-C PCR for each sample, indicating non-specific amplification in HLA-C PCR with off-target primer binding. It was concluded that it may not be feasible to eliminate all DNA during RNA extraction using the RNA extraction kit in this assay. Consequently, this significantly affected the downstream assay results of ddPCR due to non-specific quantification of non-EBNA-1 DNA products. However, the existence of DNA in the RNA samples was not a crucial inhibitor of qPCR specificity.

In theory, if the purity of RNA was very high, the DNA copy number could be determined from the original sample PBMC count and related to the concentration of RNA as determined by Nanodrop spectrophotometry (see 11.2 Methods). However, the Nanodrop could not be used to analyse RNA extraction products for quantification due to the impurity of the RNA (absorbance ratio of 1.70) and the spectrophotometer inaccuracy at concentrations less than 40µg/mL. Improvement of the RNA purity by further increasing the number of DNA digestion steps, was not anticipated. As an alternative option to the Nanodrop, the use of Agilent 2100 Bioanalyzer for RNA quantification was speculated to be a more accurate technique. The bioanalyzer uses the fluorescence of RNA molecules in a microfluidic chip to determine the size and mass of the product. However, an RNA reference standard and a microfluidics chip would be required and could not be tested within the time frame of this project.

The reverse-transcription of RNA into cDNA was initially tested using random hexamers as well as oligo dT primers in this assay. Early in testing, it was determined that oligo dT primers successfully supported reverse-transcription of RNA, whereas random hexamers failed. Hence, oligo dT primers were utilized in reverse-transcription for the remainder of RNA sample conversions. Failure of the random hexamers may be due to how they

prime at random on RNA, resulting in small segments of cDNA that may not include the full target EBNA-1 segment (850bp for ddPCR primers and 97bp for qPCR primers). Contrastingly, oligo dT primers start at the poly-A tail of RNA, where reverse transcriptase also starts, and result in far larger segments. Consequently, oligo dT primers were utilized to reverse transcribe cDNA templates for the downstream assays of ddPCR and qPCR.

13.1.2 Investigation of ddPCR results

During ddPCR testing of two healthy control samples, the ddPCR reader did not quantify EBNA-1, but successfully detected one LCL sample and the Daudi positive control dilutions 1:1000 and 1:10,000. This assay would need to be repeated for confirmation, but it can be concluded that the negative results indicate the EBNA-1 DNA copy numbers in the healthy control samples were too low for the ddPCR reader to detect. Hence, the technique was determined to not be sensitive enough, considering the positive control, Daudi, was detected by ddPCR. The detection limit for ddPCR was determined to be 282 EBNA-1 DNA copies, as detected in the Daudi dilution of 1:10,000. Contrastingly, previous studies demonstrated ddPCR to be a sensitive method for EBNA-1, with a limit of detection at 3.12 $\log_{10}$ copies/mL (129). Nevertheless, next to the low sensitivity found in this assay, poor specificity for the target EBNA-1 gene amplification was demonstrated. Despite the aforementioned genomic DNA present in the RNA samples, it was predicted amplification and quantification of the target EBNA-1 would be successful as a result of the reduced amount of DNA. However, one of the two LCL positive controls in early testing proved this was not the case as double bands (~850bp and 500bp) were observed on agarose gel after ddPCR amplification. It was later confirmed by the negative EBNA-1 sequencing results that the ddPCR EvaGreen dye and in-house primers were not specific for EBNA-1 alone. As non-specific amplification would still be quantified by ddPCR, this method was unsuitable for further use with the current procedure.

A possible improvement of the ddPCR assay may be to use the qPCR primers and probe with the ddPCR reader, a probe-specific master mix and ddPCR probe oil instead of DNA-specific EvaGreen Supermix. Previous research has found ddPCR to be an accurate method of EBNA-1 quantification (129) however it has also been confirmed previously to be no more accurate than qPCR (117). Due to time and resource constraints, repeating the assay with different primers and probe was not pursued in the confines of this experiment.

13.2 Analysis of quantitative PCR (qPCR)

13.2.1 Investigation of qPCR results

Using RNA as a template for cDNA was proposed to reduce the likelihood of non-specific amplification, as the alanine-glycine rich region in EBNA-1 is homologous with multiple sites on the human genome (69). Despite the presence of DNA in the RNA samples, the qPCR technique was 100% EBV specific and the qPCR reader did not detect non-specific amplification; only the correctly amplified target of 97bp EBNA-1. This was enabled by the combination of a specific FAM probe with primers, which together are highly specific for the EBNA-1 sequence. Confirmation by agarose gel of this specificity was determined by band length corresponding to qPCR detection. Though some samples did produce fragments at lengths other than 97bp, or no fragments at all, these were not detected by qPCR. Ergo, specificity of the qPCR for EBNA-1 was established to be excellent.

Regarding the sensitivity of the qPCR technique, it was found only 31 out of 38 healthy control samples could be detected. However, while all samples were tested in triplicate, only 14 samples were successfully duplicated, and merely three samples detected in triplicate. Although not all samples could be amplified with qPCR, the limit of detection of this assay was determined to be excellent with a minimum of 5 DNA copies/2µL or 2515 DNA copies/mL, and the limit of quantification (as defined by lowest DNA copy

number in successfully replicated samples) was 52 DNA copies/2µL, or 26,000 DNA copies/mL. In comparison to previous studies (114,115), this assay was determined to be sensitive, however, this sensitivity was not reproducible for all samples. Differences in technical factors, such as choice of nucleic extraction method, target latent gene, and different qPCR thermocyclers made it difficult to directly compare the results of latent EBNA-1 quantification to aforementioned studies (114,115). As previous studies have measured the DNA copy number/mL, the comparison with the results of this study was not complete due to PBMC count variation prior to RNA extraction. Hence, whilst the detection limit was low, the reproducibility of detection was poor. A suggested improvement would be the incorporation of an automated robotic pipetting setup to minimize error and reduce variability within results.

To further support the accuracy of the primer and probe kit, the qPCR primer amplification efficiency (a rate of accurate amplification for every cycle) was determined. With a very high amplification efficiency (95.75%, as calculated in Methods) and a low difference in Cq value change (3.49 cycles) between standard dilutions, the assay was determined to be very specific. Consequently, this reinforced qPCR as an accurate assay accounting for minor variation between standards

Stochastic variation of the qPCR assay resulted in variable DNA copy numbers in the healthy control samples. For the three healthy control samples successfully tested in triplicate by qPCR, there was a very high standard deviation for the EBNA-1 DNA copy numbers (between 5.79×10^4 and 6.52×10^8 DNA copies). As a consequence, reproducibility of the sample DNA copy numbers was significantly limited. However, high standard deviation was expected, as qPCR utilizes relative fluorescence, and as such Cq values varied between assays. However, it was still considered to be absolute

quantification as a positive control standard with a known copy number was included in each assay, allowing EBNA-1 DNA copy numbers to be calculated.

Initially, the threshold used in the qPCR Bio-Rad CFX Manager software (Bio-Rad) was the default on the qPCR reader, (100 relative fluorescence units (RFU)). After the first two to three cycles of PCR, this default threshold was determined, allowing the initial non-specific amplification to be accounted for. The threshold was later determined to be 455 RFU as a consequence of early breaching by the healthy controls, and this threshold was then used for all future qPCR assays. Using an unoptimized threshold increased the possibility of inaccurate quantification due to early breaching. A number of samples were observed to breach the threshold at very low Cq values, resulting in large DNA copy numbers, such as 1.54 Cq (or >5trillion DNA copies). This occurred despite no amplification products appearing tested on an agarose gel, suggestive of a false positive. For this reason, the threshold was later raised to 455 RFU, which was determined to be above all early noise but low enough for the standard to be detected to 6.84 DNA copies. Fortunately, the threshold could be adjusted post-PCR and hence the correct quantities of EBNA-1 in these samples were successfully recorded. When the threshold was adjusted, the Cq value of the standard and the healthy control samples changed. Yet, as this study was looking at absolute quantification, not relative quantification, it was necessary to use a consistent threshold; thus, an optimized threshold was determined.

Inhibition of qPCR by sample-specific factors, biological products, and non-biological products was reduced at every step. Hindrance of the assay by biological products was limited by increasing RNA purity during RNA extraction with extended DNase treatment, and aseptic technique to eliminate contamination. Additionally, sample-specific inhibition was reduced by using the same sample source type for all qPCR assays, which was PBMCs extracted from whole blood and limited freeze-thawing. Furthermore,

possible impediment of the qPCR by non-biological compounds, such as chemical reagents, was also diminished by the multiple wash steps of the silica membrane in the RNA spin column. This ensured only nucleic acid remained on the membrane by the final step.

13.3 Analysis of flow cytometry coupled with fluorescent in situ hybridisation (flow-FISH)

Experimental testing for flow-FISH was limited by resources. The EBER probe kit only supplied enough reagents for 20 reactions. As a result, only two healthy control samples were tested by flow-FISH in triplicate after assay optimisation and control sample testing. Additionally, EBV infected cells in latency were expected to be very rare. A previous study estimated 1% of all B lymphocytes to be latently infected with EBV (130). Therefore, the decision was made to enrich B lymphocytes before testing. The enriched B lymphocyte populations were 4.65 x 10^6 cells for one sample and 11.6 x 10^6 cells for the second sample, limiting the number of times the assay could be repeated. Due to this restriction of resources, the single stains for the antibodies and probe were initially tested on healthy control PBMC populations instead of enriched B lymphocytes. As B lymphocytes are present in PBMC populations, the voltage and compensation settings would be nearly identical.

For experimental optimisation, the voltage for the flow cytometer was adjusted in single stained tubes and compensation was calculated. The voltage was adjusted to allow distinction between positive and negative populations within the measurable window. However, positive and negative distinctions in the single stains relied on the presence of positive populations, high binding affinity of the antibody/probe and a negative unstained population. As enriched B lymphocytes were used there were no negative cells present to

serve as a control. Without a truly positive population to compare against the negative, it was very difficult to confirm if the population was positive. The experiment was therefore repeated using PBMCs to help with the initial voltage adjustments and gating strategy. A number of positive and negative populations were easier to distinguish based on the antibody used. For example, positive populations of B lymphocytes with surface markers CD20, IgD, and CD38, could be more clearly discriminated compared to those with very minimal positive shift, such as CD19, CD24, and CD27. This small shift was suspected to be attributable to antibody-specific factors such as resolution, spillover and target affinity. Resolution influences the brightness of fluorophores, and it is known that BV421, BV510, PE and PE-Cy7 fluorochromes (for anti-CD38, anti-CD27, anti-CD19, and anti-IgD, respectively) are very bright. However, this was inconclusive as anti-CD19 was labelled with PE and anti-CD27 was labelled with BV510, both of which are very bright fluorophores, yet these antibodies were difficult to distinguish from negative populations. When compared to moderate or dim fluorophores, such as FITC and APC-HC for EBER and anti-CD20 respectively, brighter fluorophore events are more readily detectable than dimmer ones, which can affect quantification and measurement. This may have influenced the very high number of events detected for the anti-CD38/BV421 and anti-IgD/PE-Cy7 antibodies compared to others. Due to this uncertainty in positive shift, it was difficult to determine an absolute quantification for B lymphocyte subset events.

Investigation of the flow-FISH output for EBER-positive healthy control cells was successfully determined using Kaluza software to distinguish positive populations from negative populations. However, difficulties arose as a result of the low number of positive events for surface antibody and EBER probe targets, which caused only a slight positive shift and made gating difficult. To aid in distinguishing the positive and negative populations for EBER, the populations were compared by overlaying the positive over the negative population using Kaluza software. Further, to ensure an accurate

representation for both populations, the flow events were gated so there were equal number of cells in each population. With this overlay, the positive population was distinguished by the slight shift to the right in comparison to the negative population.

As aforementioned, the most significant limitation of flow-FISH was determined to be the low binding affinity of anti-CD19 in the presence of the EBER probe, which prevented the phenotyping of memory B lymphocytes, and subsequently inhibited the analysis of EBER in memory B lymphocytes. To troubleshoot the antibody, anti-CD19 was tested as a single stain immediately after fixation without proceeding to the permeabilization and hybridization steps, and it was determined that the anti-CD19 antibody functioned in the absence of these protocols. However, it was inconclusive whether this was due to the permeabilization step, the EBER probe hybridization step, or how these techniques may have affected the antibody surface marker. Availability of CD19 surface markers may have been altered by these techniques and the low binding affinity of anti-CD19 may be attributable to the process of fixation and permeabilisation. An improvement could be to optimise the anti-CD19 antibody for use in conjunction with the EBER probe technique. Possible adjustments could include increased anti-CD19 concentration, longer staining times, or an alternative fluorophore to be attached to anti-CD19.

Gating of EBER-positive naïve B lymphocytes, and their non-class switched memory B lymphocyte derivatives, was enabled by the population shift of positive EBER cell populations. Naïve B lymphocytes and non-class switched memory B lymphocytes may have had a positive result as a consequence of the nature of EBV latency: EBV is known to reactivate and exit latency, however the underlying mechanism is unknown (105). EBV reactivation could potentially increase the capacity of EBV to infect naïve B lymphocytes, thus reinitiating the cycle. Consequentially, naïve B lymphocytes are forced into transition by EBV to become memory B lymphocytes (105). Re-activation of EBV is a

potential explanation for the presence of EBER RNA in naïve non-class switched memory B lymphocytes.

In an individual with latent EBV infection, it was expected that memory B lymphocytes would be the B lymphocyte subset with the highest level of EBER. Previously, studies have found EBV to persist latently in memory B lymphocytes after acute infection has ceased (131). However, aforementioned studies have only determined EBER presence in lytic infection or EBV-transformed cell lines using flow-FISH, but not in latency (118,119). Nonetheless, in this experiment, the memory B lymphocytes could not be gated by flow-FISH analysis as a result of low binding affinity of the anti-CD19 antibody. Therefore, it was possible the memory B lymphocytes in the samples were positive for EBER, but it was impossible to determine this from the results.

Although LCLs proved to be a suitable positive control for EBER, it required a different voltage and compensation setting from the healthy control sample. Thus, it was not possible to compare the results of the LCL positive events and the healthy control positive events directly by overlay. LCLs were a poor positive control for antibody-surface marker binding, and only very limited antibodies bound LCL surface markers. The low binding affinity may be attributed to downregulated LCL surface marker expression during EBV transformation. This was not unexpected, but due to time constraints, a more effective substitute for LCLs was not determined. As surface marker and EBER expression is variable between PBMC, enriched B lymphocytes, and LCL populations, flow cytometric analysis was not directly comparable. For the reason that cell populations were detected at different positions, it was not possible to overlay each for a direct comparison of positive EBER populations. As a result, suitability of the LCL positive for confirmation of the EBER probe function in this assay was established, however it was determined to be unsuitable for B lymphocyte surface marker validation.

Originally, the gating strategy used in this flow cytometry assay was designed by Dr. Monika Tschochner to be inclusive of a CD45 antibody labelled with a FITC fluorophore. CD45 is a universal lymphocyte surface marker and would have been highly suitable for gating lymphocytes such as memory B lymphocytes. However, the EBER probe was labelled with FITC and hence the antibody was swapped for the probe. As the gating strategy was already limited by the low binding affinity of anti-CD19, the gating of some B lymphocyte subsets such as memory B lymphocytes (CD45+, CD19+, CD27+), was more challenging in the absence of anti-CD45. An additional improvement to the gating strategy would be to adjust the flow panel to include an additional marker, such as $CD138^{+}$ in the panel to help in detecting plasmablasts.

Altogether, flow-FISH proved to be sensitive and specific enough to detect EBV-positive B lymphocyte subsets, however the protocol needs to be further modified to enable reliable detection of all B lymphocyte subsets in sufficient quantity.

13.4 Future directions

Presently, qPCR and flow-FISH have been determined to be successful in specifically detecting EBV infected lymphocytes. In future research, the qPCR technique will need to be further optimised, particularly to improve reproducibility and reduce variability. qPCR variability can be attributed to many factors, but human error can be diminished if pipetting is in a non-manual platform such as a robotic pipetting machine. At this point, qPCR has only been sensitive enough to detect latently infected cells in a majority of healthy control samples. It is uncertain if qPCR is suitable for the detection of EBNA-1 in B lymphocyte subpopulations, where it is predicted the EBNA-1 copy number will be further reduced. To overcome this, blood samples could be collected with increased cell counts.

One of the major caveats of the flow-FISH technique was the interference of the EBER probe protocol with the anti-CD19 antibody. The flow-FISH technique would be improved with the use of a different fluorochrome-coupled anti-CD19 antibody, or by using an alternative marker to CD19 to distinguish memory B lymphocytes and plasmablasts in B lymphocyte phenotyping.

Once the B lymphocyte subset phenotyping is confirmed, the MS patient samples could be analysed using flow-FISH for determination of a ratio between EBER-positive B lymphocyte types compared to healthy controls.

Ideally, after both qPCR and flow-FISH techniques are optimized, B lymphocytes could be enriched and then flow sorted according to their surface antigen expression. Hence, the B lymphocyte subsets could be separately analysed using qPCR for confirmation of EBNA-1 quantities within each subset.

Upcoming research will be commenced with testing MS patient samples at different disease stages to elucidate EBV quantities in different B lymphocyte subsets. These quantities will be compared between acute and early MS, relapsing remitting MS (with and without acute symptoms), primary-progressive MS, patients without symptoms over 10 years (benign MS), and healthy control samples.

In the expectation of identifying an EBV infected B lymphocyte subset, the additional surface marker, or combination of surface markers indicative of EBV infected B lymphocytes will be characterized. Subsequently, the predicted surface marker or combination of surface markers will enable flow sorting of the target EBV infected B lymphocyte subset. Therefore, live cells can be harvested, and fixation protocols can be avoided, enabling further phenotyping of their antigen-presenting cell characteristics. For determination of MHC characteristics and antigen-related behaviour in this B lymphocyte subset, they would be exposed to T lymphocytes from MS patients and healthy controls.

In addition, B lymphocyte depletion therapy could utilize the determined EBV-infected B lymphocyte subset in MS patients as a target for a new therapeutical approach. Currently, B lymphocyte depletion therapy targets all CD20 lymphocytes, which are the majority of all B lymphocytes (45). Depletion of all B lymphocytes can cause some adverse side effects, such as allergic reactions and infections (45). This therapy could be modified to be more specific, based on the EBV-infected B lymphocyte subset population to be determined, in such a way that a surface marker cocktail would only deplete the target population rather than all B lymphocytes. Subsequently, MS patients would experience less adverse side effects as only a minor proportion of lymphocytes would be depleted. Trialled clinically, this treatment could further confirm the association between EBV and MS through the depletion of the virus' most prominent carrier.

Thus, the research initiated in this project could progress to enable the confirmation of a biomarker for MS patients as well as an objective for B lymphocyte depletion therapy. Although there is some further research required to reach this aim, future therapy for MS patients with reduced side effects as a result of targeted EBV infected B cell depletion is an objective in sight.

14 Conclusion

This is the first reported study of quantification of EBV in latency, targeting EBNA-1 and EBER in healthy control samples, using a combination of ddPCR, qPCR and flow-FISH. In conclusion, comparison of these three assays identified ddPCR as unsuitable with its current protocol for accurate EBV quantification.

Contrastingly, qPCR was ascertained to be 100% specific for EBNA-1 and very sensitive, allowing accurate quantification in latency with as little as ~52 DNA copies. However, significant variation between healthy control sample DNA copy numbers was observed in samples tested in triplicate and this disparity will have to be overcome. Despite this, qPCR was still proven to be a technique with absolute quantification, due to the reproducibility of the standard DNA detection.

Furthermore, the novel flow-FISH technique successfully detected EBER in 28-38% of healthy control B lymphocytes. Sensitivity of this method was verified when testing an enriched B lymphocyte population, as it increased the likelihood of EBER detection. EBER was found to be in greatest proportions in naïve B lymphocytes and non-class switched memory B lymphocytes, which was in contrast to current literature, as memory B lymphocytes were identified to be EBV infected when testing LCLs. Of note, LCLs are known to behave contrarily to enriched B lymphocyte populations and resemble the characteristics of cancer cells, including altered cell surface marker expression. Interestingly, whilst transformation of B lymphocytes into LCLs is initiated by EBV, several studies observed that LCLs often do not harbour the EBV genome after passage or clonal expansion in patient cells. Low detection of memory B lymphocytes was attributed to the low binding affinity of anti-CD19 antibody in the presence of EBER, hence it cannot be ruled out that memory B lymphocytes represent the B lymphocyte subset with the highest EBER copy number.

The quantification of EBNA-1 in healthy control samples is an essential step and will be optimized in future studies. In addition, further research will enable more insight to be gained into the role of EBV infected B lymphocyte subsets in the context of MS. This will enable characterization of EBV infected B lymphocyte subsets and hopefully culminates in a surface marker panel to be utilized as a biomarker for MS in the future. Current MS therapies, especially B lymphocyte depletion, could be improved with specific targeting of surface markers based on the methods utilized in this project. Specific B lymphocyte subpopulation depletion would reduce adverse side effects with a more target approach. In addition, the surface marker panel may also serve as a biomarker of MS before the initial symptoms occur. This exciting research could potentially significantly reduce disease burden and improve patient outlook and quality of life.

15 References

1. Schwarz A, Balint B, Korporal-Kuhnke M, Jarius S, von Engelhardt K, Fürwentsches A, et al. B-cell populations discriminate between pediatric- and adult-onset multiple sclerosis. Neurology [serial online]. 2017 [cited 2018 Jan 6];4(1):309. Available from: http://nn.neurology.org

2. Corcione A, Casazza S, Ferretti E, Giunti D, Zappia E, Pistorio A, et al. Recapitulation of B cell differentiation in the central nervous system of patients with multiple sclerosis. Proc Natl Acad Sci U S A [serial online]. 2004 [cited 2018 Jan 6];101(30):11064–9. Available from: http://www.ncbi.nlm.nih.gov/pubmed/

3. Serafini B, Severa M, Columba-Cabezas S, Rosicarelli B, Veroni C, Chiappetta G, et al. Epstein-Barr virus latent infection and BAFF expression in B cells in the multiple sclerosis brain: implications for viral persistence and intrathecal B-cell activation. J Neuropathol Exp Neurol. 2010;69(7):677–93.

4. Alotaibi S, Kennedy J, Tellier R, Stephens D, Banwell B. Epstein-Barr virus in pediatric multiple sclerosis. Jama. 2004;291(15):1875–9.

5. Haahr S, Plesner AM, Vestergaard BF, Höllsberg P. A role of late Epstein-Barr virus infection in multiple sclerosis. Acta Neurol Scand. 2004;109(4):270–5.

6. Castellazzi M, Contini C, Tamborino C, Fasolo F, Roversi G, Seraceni S, et al. Epstein-Barr virus-specific intrathecal oligoclonal IgG production in relapsing-remitting multiple sclerosis is limited to a subset of patients and is composed of low-affinity antibodies. J Neuroinflammation [serial online]. 2014 [cited 2018 Jan 6];11(1):188. Available from: http://jneuroinflammation.biomedcentral.com

7. Franciotta D, Di Stefano AL, Jarius S, Zardini E, Tavazzi E, Ballerini C, et al.

Cerebrospinal BAFF and Epstein-Barr virus-specific oligoclonal bands in multiple sclerosis and other inflammatory demyelinating neurological diseases. J Neuroimmunol [serial online]. 2011 [cited 2018 Jan 6];230(1–2):160–3. Available from: http://dx.doi.org

8. Zhou Y, Simpson Jr S, Charlesworth JC, Van Der Mei I, Lucas R, Ponsonby AL, et al. Variation within myelin basic protein gene predicts disease course in multiple sclerosis. Mult Scler. 2015;23(11 Supp.):80.

9. Lünemann JD, Jelcić I, Roberts S, Lutterotti A, Tackenberg B, Martin R, et al. EBNA1-specific T cells from patients with multiple sclerosis cross react with myelin antigens and co-produce IFN-gamma and IL-2. J Exp Med [serial online]. 2008 [cited 2018 Jan 6];205(8):1763–73. Available from: http://www.pubmedcentral.nih.gov

10. Ramasamy R, Joseph B, Whittall T. Potential molecular mimicry between the human endogenous retrovirus W family envelope proteins and myelin proteins in multiple sclerosis. Immunol Lett [serial online]. 2017 [cited 2018 Jan 6];183:79–85. Available from: http://linkinghub.elsevier.com

11. Lomakin YA, Zakharova MY, Belogurov AA, Bykova NA, Dronina MA, Tupikin AE, et al. Polyreactive monoclonal autoantibodies in multiple sclerosis: Functional selection from phage display library and characterization by deep sequencing analysis. Acta Naturae. 2013;5(19):94–104.

12. Gabibov A. Exposure to the Epstein–Barr Viral Antigen Latent Membrane Protein 1 Induces Myelin-Reactive Antibodies In Vivo. 2017;8(7):1–11.

13. Chaganti S, Heath EM, Bergler W, Kuo M, Buettner M, Niedobitek G, et al. Epstein-Barr virus colonisation of tonsillar and peripheral blood B cell subsets in

primary infection and persistence. Blood [serial online]. 2009 [cited 2018 Jan 6];113(25):6372–82. Available from: http://www.ncbi.nlm.nih.gov

14. Kuhlmann T, Lingfeld G, Bitsch A, Schuchardt J, Brück W. Acute axonal damage in multiple sclerosis is most extensive in early disease stages and decreases over time. Brain. 2002;125(10):2202–12.

15. Bjartmar C, Kinkel RP, Kidd G, Rudick RA, Trapp BD. Axonal loss in normal-appearing white matter in a patient with acute MS. Neurol [serial online]. 2001 [cited 2018 Jan 6];57(7):1248–52. Available from: http://www.neurology.org

16. Geurts JJG, Wolswijk G, Bö L, Van der Valk P, Polman CH, Troost D, et al. Altered expression patterns of group I and II metabotropic glutamate receptors in multiple sclerosis. Brain. 2003;126(8):1755–66.

17. Kornek B, Storch MK, Bauer J, Djamshidian A, Weissert R, Wallstroem E, et al. Distribution of a calcium channel subunit in dystrophic axons in multiple sclerosis and experimental autoimmune encephalomyelitis. Brain. 2001;124(6):1114–24.

18. Trapp BD, Peterson J, Ransohoff RM, Rudick R, Mörk S, Bö L. Axonal transection in the lesions of Multiple Sclerosis. N Engl J Med [serial online]. 1998 [cited 2018 Jan 6];338(5):278–85. Available from: http://www.nejm.org

19. Ferguson B, Matyszak MK, Esiri MM, Perry VH. Axonal damage in acute multiple sclerosis lesions. Brain. 1997;120(3):393–9.

20. Scalfari A, Neuhaus A, Degenhardt A, Rice GP, Muraro PA, Daumer M, et al. The natural history of multiple sclerosis, a geographically based study 10: Relapses and long-term disability. Brain. 2010;133(7):1914–29.

21. Ng A V, Castro M, Weiner MW, Gelinas D, Dudley GA, Miller RG, et al. Strength, skeletal muscle composition, and enzyme activity in multiple sclerosis. J Appl Physiol. 1997;83(6):1998–2004.

22. Finlayson ML, Peterson EW, Cho CC. Risk Factors for Falling Among People Aged 45 to 90 Years With Multiple Sclerosis. Arch Phys Med Rehabil. 2006;87(9):1274–9.

23. Hirst C, Swingler R, Compston DA, Ben-Shlomo Y, Robertson NP. Survival and cause of death in multiple sclerosis: a prospective population-based study. J Neurol Neurosurg Psychiatry [serial online]. 2008 [cited 2018 Jan 6];79(9):1016–21. Available from: http://www.ncbi.nlm.nih.gov/pubmed

24. Hampshire-araújo F, Bergmann A, Maria R, Alvarenga P, Cristina C, Vasconcelos F. Malignant multiple sclerosis : clinical and demographic prognostic factors. Arq Neuropsiquiatr. 2016;75(3):139–41.

25. Confavreux C, Aimard G, Devic M. Course and prognosis of multiple sclerosis assessed by the computerized data processing of 349 patients. Brain [serial online]. 1980 [cited 2018 Jan 6];103(2):281–300. Available from: http://ovidsp.ovid.com

26. Poser CM, Paty DW, Scheinberg L. New diagnostic criteria for multiple sclerosis: Guidelines for research protocols. Ann Neurol [serial online]. 1983 [cited 2018 Jan 6];13(3):227–31. Available from: http://www.scopus.com

27. Miller DH, Chard DT, Ciccarelli O. Clinically isolated syndromes. Lancet Neurol [serial online]. 2012;11(2):157–69. Available from: http://dx.doi.org

28. Barkhof F Miller DH, Scheltens P, Campi A, Polman CH FM. Comparison of MRI criteria at first presentation to predict conversion to clinically definite

multiple sclerosis. Brain. 1997;120(11):2059–69.

29. Kurtzke JF. Rating neurologic impairment in multiple sclerosis: An expanded disability status scale (EDSS) . Neurol [serial online]. 1983 [cited 2018 Jan 6];33(11):1444. Available from: http://www.neurology.org

30. Jacobs LD, Beck RW, Simon JH, Kinkel RP, Brownscheidle CM, Murray TJ, et al. Intramuscular interferon beta-1a therapy initiated during a first demyelinating event in multiple sclerosis. N Engl J Med. 2000;343(13):898–904.

31. Li DKB, Duquette P, Girard M, Despault L, DuBois R, Knobler RL, et al. Interferon beta-1b is effective in relapsing-remitting multiple sclerosis: I. Clinical results of a multicenter, randomized, double-blind, placebo-controlled trial. Neurology [serial online]. 1993 [cited 2018 Jan 6];43(4):655–655. Available from: http://www.neurology.org

32. Ziemssen T, Kümpfel T, Klinkert WEF, Neuhaus O, Hohlfeld R. Glatiramer acetate-specific T-helper 1- and 2-type cell lines produce BDNF: implications for multiple sclerosis therapy. Brain-derived neurotrophic factor. Brain. 2002;125(11):2381–91.

33. Ahn Y, Jeon S, Chang CY, Goh E, Kim SS. Glatiramer acetate attenuates the activation of CD4 + T cells by modulating STAT1 and −3 signaling in glia. Nat Publ Gr [serial online]. 2017 [cited 2018 Jan 6];(8):1–16. Available from: http://dx.doi.org

34. Comi G, Filippi M, Wolinsky JS. European/Canadian multicenter, double-blind, randomized, placebo-controlled study of the effects of glatiramer acetate on magnetic resonance imaging-measured disease activity and burden in patients with relapsing multiple sclerosis. European/Canadian Gla. Ann Neurol [serial

online]. 2001 [cited 2018 Jan 6];49(3):290–7. Available from: http://www.ncbi.nlm.nih.gov/pubmed

35. Johnson KP, Brooks BR, Cohen JA, Ford CC, Goldstein J, Lisak RP, et al. Extended use of glatiramer acetate (Copaxone) is well tolerated and maintains its clinical effect on multiple sclerosis relapse rate and degree of disability. Neurol [serial online]. 1998 [cited 2018 Jan 6];50(3):701–8. Available from: http://www.neurology.org

36. Comi G, Martinelli V, Rodegher M, Moiola L, Bajenaru O, Carra A, et al. Effect of glatiramer acetate on conversion to clinically definite multiple sclerosis in patients with clinically isolated syndrome (PreCISe study): a randomised, double-blind, placebo-controlled trial. Lancet [serial online]. 2009 [cited 2018 Jan 6];374(9700):1503–11. Available from: http://dx.doi.org

37. Mikol DD, Barkhof F, Chang P, Coyle PK, Jeffery DR, Schwid SR, et al. Comparison of subcutaneous interferon beta-1a with glatiramer acetate in patients with relapsing multiple sclerosis (the REbif vs Glatiramer Acetate in Relapsing MS Disease [REGARD] study): a multicentre, randomised, parallel, open-label trial. Lancet Neurol. 2008;7(10):903–14.

38. Sera B, Scorsi E, Rosicarelli B, Rigau V, Thouvenot E, Aloisi F. Massive intracerebral Epstein-Barr virus reactivation in lethal multiple sclerosis relapse after natalizumab withdrawal. J Neuroimmunol. 2017;307(6):14–7.

39. Castellazzi M, Delbue S, Elia F, Gastaldi M, Franciotta D, Rizzo R, et al. Epstein-Barr virus specific antibody response in multiple sclerosis patients during 21 months of natalizumab treatment. Dis Markers. 2015;2015(901312):1–5.

40. Topping J, Dobson R, Lapin S, Maslyanskiy A, Kropshofer H, Leppert D, et al.

The effects of intrathecal rituximab on biomarkers in multiple sclerosis. Mult Scler Relat Disord [serial online]. 2016 [cited 2018 Jan 6];6(1):49–53. Available from: http://dx.doi.org

41. Hawker K, O'Connor P, Freedman MS, Calabresi PA, Antel J, Simon J, et al. Rituximab in patients with primary progressive multiple sclerosis: Results of a randomized double-blind placebo-controlled multicenter trial. Ann Neurol. 2009;66(4):460–71.

42. Palanichamy A, Jahn S, Nickles D, Derstine M, Abounasr A, Hauser S, et al. Rituximab efficiently depletes increased CD20 expressing T cells in multiple sclerosis patients. J Immunol. 2014;193(2):580–6.

43. Weber MS, Prod'homme T, Patarroyo JC, Molnarfi N, Karnezis T, Lehmann-Horn K, et al. B-cell activation influences T-cell polarization and outcome of anti-CD20 B-cell depletion in central nervous system autoimmunity. Ann Neurol. 2010;68(3):369–83.

44. Barr TA, Shen P, Brown S, Lampropoulou V, Roch T, Lawrie S, et al. B cell depletion therapy ameliorates autoimmune disease through ablation of IL-6–producing B cells. J Exp Med [serial online]. 2012 [cited 2018 Jan 6];209(5):1001–10. Available from: http://www.jem.org

45. Hauser S, Waubant E, Arnold DL, Vollmer T, Antel J, Fox RJ, et al. B-Cell Depletion with Rituximab in Relapsing–Remitting Multiple Sclerosis. N Engl J Med. 2008;358(7):676–88.

46. de Flon P, Laurell K, Söderström L, Gunnarsson M, Svenningsson A. Improved treatment satisfaction after switching therapy to rituximab in relapsing–remitting MS. Mult Scler J [serial online]. 2016 [cited 2018 Jan 6];10:1–9. Available from:

http://journals.sagepub.com

47. Mouhieddine TH, Darwish H, Fawaz L, Yamout B, Tamim H, Khoury SJ. Risk factors for multiple sclerosis and associations with anti-EBV antibody titers. Clin Immunol [serial online]. 2015 [cited 2018 Jan 6];158(1):59–66. Available from: http://dx.doi.org

48. Nolan D, Castley A, Tschochner M, James I, Qiu W, Sayer D, et al. Contributions of vitamin D response elements and HLA promoters to multiple sclerosis risk. Neurology. 2012;79(6):538–46.

49. Lindsey, J. William, DeGannes SL, Pate KA, Zhao X. Antibodies specific for Epstein-Barr virus nuclear antigen-1 cross-react with human heterogeneous nuclear ribonucleoprotein L. 2016;8(5):583–92.

50. Strautins K, Tschochner M, James I, Choo L, Dunn DS, Pedrini M, et al. Combining HLA-DR risk alleles and anti-Epstein-Barr virus antibody profiles to stratify multiple sclerosis risk. Mult Scler J [serial online]. 2013 [cited 2018 Jan 6];20(3):286–94. Available from: http://dx.doi.org

51. Xiao D, Ye X, Zhang N, Ou M, Guo C, Zhang B, et al. A meta-analysis of interaction between Epstein-Barr virus and HLA-DRB1*1501 on risk of multiple sclerosis. Sci Rep [serial online]. 2015 [cited 2018 Jan 6];5(601):18083. Available from: http://www.ncbi.nlm.nih.gov/pubmed

52. Debouverie M, Pittion-Vouyovitch S, Louis S, Roederer T, Guillemin F. Increasing incidence of multiple sclerosis among women in Lorraine, Eastern France. Mult Scler J [serial online]. 2007 [cited 2018 Jan 6];13(8):962–7. Available from: http://journals.sagepub.com

53. Moldovan IR, Cotleur AC, Zamor N, Butler RS, Pelfrey CM. Multiple sclerosis

patients show sexual dimorphism in cytokine responses to myelin antigens. J Neuroimmunol. 2008;193(1–2):161–9.

54. Mizuno M, Noto D, Kaga N, Chiba A, Miyake S. The dual role of short fatty acid chains in the pathogenesis of autoimmune disease models. PLoS One. 2017;1–15.

55. Agranoff BW, Goldberg D. Diet and the geographical distribution of Multiple Sclerosis. Lancet [serial online]. 1974 [cited 2017 Oct 24];304(7888):1061–6. Available from: http://www.sciencedirect.com

56. Hammond SR, English DR, McLeod JG. The age-range of risk of developing multiple sclerosis: evidence from a migrant population in Australia. Brain. 2000;123(1):968–74.

57. Lindsey J, Dooley M. The antibody response to Epstein-Barr Virus in Multiple Sclerosis is increased only to selected antigens. Neurology [serial online]. 2016 [cited 2018 Jan 6];86(16):5. Available from: http://www.neurology.org

58. Lauer K. Ecologic studies of multiple sclerosis. Neurology [serial online]. 1997 [cited 2018 Jan 6];49(2 Supp 2):18–26. Available from: http://www.neurology.org

59. World Health Organisation. Atlas Multiple Sclerosis Resources in the World [document on the Internet]. MS Atlas. 2008. Available from: http://www.who.int/mental_health/neurology/Atlas_MS_WEB.pdf

60. McLeod JG, Hammond SR, Hallpike JF. Epidemiology of multiple sclerosis in Australia with NSW and SA survey results. Med J Aust [serial online]. 1994 [cited 2018 Jan 6];160(3):117–22. Available from: http://europepmc.org

61. O'Connell K, Hutchinson M, Tubridy N, McGuigan C. Incidence of multiple

sclerosis in the Republic of Ireland: an observational population-based study. Mult Scler Relat Disord [serial online]. 2015 [cited 2018 Jan 6];13(1):75–80. Available from: http://dx.doi.org

62. Grytten N, Torkildsen Ø, Myhr K-M. Time trends in the incidence and prevalence of multiple sclerosis in Norway during eight decades. Acta Neurol Scand [serial online]. 2015 [cited 2018 Jan 6];132(199):29–36. Available from: http://doi.wiley.com

63. Kurtzke JF. Multiple sclerosis in time and space-geographic clues to cause. J Neurovirol. 2000;6 Supp 2(3):134–40.

64. Sawcer S, Hellenthal G, Pirinen M, Spencer CCA, Patsopoulos NA, Moutsianas L, et al. Genetic risk and a primary role for cell-mediated immune mechanisms in multiple sclerosis. Nature. 2012;476(7359):214–9.

65. Sundqvist E, Sundström P, Lindén M, Hedström AK, Aloisi F, Hillert J, et al. Epstein-Barr virus and multiple sclerosis: interaction with HLA. Genes Immun [serial online]. 2012 [cited 2018 Jan 6];13(1):14–20. Available from: http://www.ncbi.nlm.nih.gov/pubmed

66. Burrell A, Handel AE, Ramagopalan S, Ebers GC, Morahan J. Epigenetic mechanisms in Multiple Sclerosis and the Major Histocompatibility Complex (MHC). Discov Med. 2011;11(58):187–96.

67. Lang HLE, Jacobsen H, Ikemizu S, Andersson C, Harlos K, Madsen L, et al. A functional and structural basis for TCR cross-reactivity in multiple sclerosis. Nat Immunol [serial online]. 2002 [cited 2018 Jan 6];3(10):940–3. Available from: http://dx.doi.org

68. Holmøy T, Kvale EØ, Vartdal F. Cerebrospinal fluid CD4 $^{+}$ T cells from a

multiple sclerosis patient cross-recognize Epstein-Barr virus and myelin basic protein. J Neurovirol [serial online]. 2004 [cited 2018 Jan 6];10(5):278–83. Available from: http://link.springer.com

69. Tschochner M, Leary S, Cooper D, Strautins K, Chopra A, Clark H, et al. Identifying Patient-Specific Epstein-Barr Nuclear Antigen-1 Genetic Variation and Potential Autoreactive Targets Relevant to Multiple Sclerosis Pathogenesis. PLoS One [serial online]. 2016 [cited 2018 Jan 6];11(2):1–22. Available from: http://dx.doi.org

70. Pender MP. Infection of autoreactive B lymphocytes with EBV, causing chronic autoimmune diseases. Trends Immunol. 2003;24(11):584–8.

71. Knopf PM, Harling-Berg CJ, Cserr HF, Basu D, Sirulnick EJ, Nolan SC, et al. Antigen-dependent intrathecal antibody synthesis in the normal rat brain: tissue entry and local retention of antigen-specific B cells. J Immunol [serial online]. 1998 [cited 2018 Jan 6];161(2):692–701. Available from: http://www.ncbi.nlm.nih.gov/pubmed

72. Baker D, Marta M, Pryce G, Giovannoni G, Schmierer K. Memory B cells are major targets for effective immunotherapy in relapsing Multiple Sclerosis. EBioMedicine [serial online]. 2017 [cited 2018 Jan 6];16:41–50. Available from: http://linkinghub.elsevier.com

73. Lünemann JD, Edwards N, Muraro PA, Hayashi S, Cohen JI, Münz C, et al. Increased frequency and broadened specificity of latent EBV nuclear antigen-1-specific T cells in multiple sclerosis. Brain. 2006;129(6):1493–506.

74. Paroni M, Maltese V, De Simone M, Ranzani V, Larghi P, Fenoglio C, et al. Recognition of viral and self-antigens by TH1 and TH1/TH17 central memory

cells in patients with multiple sclerosis reveals distinct roles in immune surveillance and relapses. J Allergy Clin Immunol [serial online]. 2017 [cited 2018 Jan 6];1–12. Available from: http://dx.doi.org

75. Harp CT, Ireland S, Davis LS, Remington G, Cassidy B, Cravens PD, et al. Memory B cells from a subset of treatment-naïve relapsing- remitting multiple sclerosis patients elicit CD4+ T-cell proliferation and IFN -γ production in response to MBP and MOG. Eur J Immunol [serial online]. 2010 [cited 2018 Jan 6];40(10):2942–56. Available from: http://onlinelibrary.wiley.com

76. Michel L, Touil H, Pikor NB, Gommerman JL, Prat A, Bar-Or A. B cells in the multiple sclerosis central nervous system: Trafficking and contribution to CNS-compartmentalized inflammation. Front Immunol. 2015;6(12):1–12.

77. Toso C, Edgar R, Pawlick R, Emamaullee J, Merani S, Dinyari P, et al. Effect of different induction strategies on effector, regulatory and memory lymphocyte sub-populations in clinical islet transplantation. Transpl Int. 2009;22(2):182–91.

78. Casiraghi C, Márquez AC, Shanina I, Horwitz MS. Latent virus infection upregulates CD40 expression facilitating enhanced autoimmunity in a model of multiple sclerosis. Nat Publ Gr [serial online]. 2015 [cited 2018 Jan 6];5(2):13995. Available from: http://www.ncbi.nlm.nih.gov/pubmed

79. Cepok S, Zhou D, Srivastava R, Nessler S, Stei S, Büssow K, et al. Identification of Epstein-Barr virus proteins as putative targets of the immune response in multiple sclerosis. J Clin Invest [serial online]. 2005 [cited 2018 Jan 6];115(5):1352–60. Available from: http://www.pubmedcentral.nih.gov

80. Matsuura H, Kirschner AN, Longnecker R, Jardetzky TS. Crystal structure of the Epstein-Barr virus (EBV) glycoprotein H/glycoprotein L (gH/gL) complex. Proc

Natl Acad Sci [serial online]. 2010 [cited 2018 Jan 6];107(52):22641–6. Available from: http://www.pnas.org

81. Szakonyi G, Klein MG, Hannan JP, Young KA, Ma RZ, Asokan R, et al. Structure of the Epstein-Barr virus major envelope glycoprotein. Nat Struct Mol Biol [serial online]. 2006 [cited 2018 Jan 6];13(11):996–1001. Available from: http://dx.doi.org

82. Tardif M, Savard M, Flamand L, Gosselin J. Impaired protein kinase C activation/translocation in Epstein-Barr virus-infected monocytes. J Biol Chem. 2002;277(27):24148–54.

83. Severa M, Giacomini E, Gafa V, Anastasiadou E, Rizzo F, Corazzari M, et al. EBV stimulates TLR- and autophagy-dependent pathways and impairs maturation in plasmacytoid dendritic cells: Implications for viral immune escape. Eur J Immunol. 2013;43(1):147–58.

84. Gross a. J, Hochberg D, Rand WM, Thorley-Lawson D a. EBV and Systemic Lupus Erythematosus: A New Perspective. J Immunol [serial online]. 2005 [cited 2018 Jan 6];174(11):6599–607. Available from: http://www.jimmunol.org

85. Erre GL, Mameli G, Cossu D, Muzzeddu B, Piras C, Paccagnini D, et al. Increased Epstein-Barr virus DNA load and antibodies against EBNA1 and EA in Sardinian patients with rheumatoid arthritis. Viral Immunol [serial online]. 2015 [cited 2018 Jan 6];28(7):385–90. Available from: http://www.ncbi.nlm.nih.gov/pubmed

86. Sundström P, Juto P, Wadell G, Hallmans G, Svenningsson A, Nyström L, et al. An altered immune response to Epstein-Barr virus in multiple sclerosis: A prospective study. Neurol [serial online]. 2004 [cited 2018 Jan 6];62(12):2277–

82. Available from: http://www.neurology.org

87. Pfuhl C, Oechtering J, Rasche L, Gieß RM, Behrens JR, Wakonig K, et al. Association of serum Epstein-Barr nuclear antigen-1 antibodies and intrathecal immunoglobulin synthesis in early multiple sclerosis. J Neuroimmunol [serial online]. 2015 [cited 2018 Jan 6];285:156–60. Available from: http://dx.doi.org

88. Serafini B, Rosicarelli B, Franciotta D, Magliozzi R, Reynolds R, Cinque P, et al. Dysregulated Epstein-Barr virus infection in the multiple sclerosis brain. J Exp Med [serial online]. 2007 [cited 2018 Jan 6];204(12):2899–912. Available from: http://www.pubmedcentral.nih.gov

89. Willis SN, Stadelmann C, Rodig SJ, Caron T, Gattenloehner S, Mallozzi SS, et al. Epstein-Barr virus infection is not a characteristic feature of multiple sclerosis brain. Brain. 2009;132(12):3318–28.

90. Zivadinov R, Cerza N, Hagemeier J, Carl E, Badgett D, Ramasamy DP, et al. Humoral response to EBV is associated with cortical atrophy and lesion burden in patients with MS. Neurology [serial online]. 2016 [cited 2018 Jan 6];3(1):190. Available from: http://www.pubmedcentral.nih.gov

91. Latham LB, Lee MJ, Lincoln JA, Ji N, Forsthuber TG, Lindsey JW. Antivirus immune activity in multiple sclerosis correlates with MRI activity. Acta Neurol Scand. 2016;133(1):17–24.

92. Sadovnick AD, Ebers GC, Dyment DA, Risch NJ. Evidence for genetic basis of multiple sclerosis. Lancet. 1996;347(9017):1728–30.

93. Qin Y, Zhang Y, Talbot P, Poole R, Antel J. Clonal expansion and somatic mutation of VH genes of B cells from the cerebrospinal fluid of multiple sclerosis. J Neuroimmunol. 1998;90(1):77.

94. Straus MSE, Cohen DJI. Epstein-Barr Virus Infections: Biology, Pathogenesis, and Management. NIH Conf. 1993;118(1):45–58.

95. Mechelli R, Anderson J, Vittori D, Coarelli G, Annibali V, Cannoni S, et al. Epstein–Barr virus nuclear antigen-1 B-cell epitopes in multiple sclerosis twins. Mult Scler J [serial online]. 2011 [cited 2018 Jan 6];17(11):1290–4. Available from: http://dx.doi.org

96. Martyn C, Cruddas M, Compston DAS. Symptomatic Epstein-Barr virus infection and multiple sclerosis. J Neurol Neurosurg Psychiatr. 1993;56:167–8.

97. Pender MP, Csurhes PA, Burrows JM, Burrows SR. Defective T-cell control of Epstein – Barr virus infection in multiple sclerosis. Nat Publ Gr [serial online]. 2017 [cited 2018 Jan 6];5(1):126–17. Available from: http://dx.doi.org

98. Pender MP, Csurhes PA, Pfluger CM, Burrows SR. Deficiency of CD8 $^{+}$ effector memory T cells is an early and persistent feature of multiple sclerosis. Mult Scler J [serial online]. 2014 [cited 2018 Jan 6];20(14):1825–32. Available from: http://journals.sagepub.com

99. van Nierop GP, Janssen M, Mitterreiter JG, van de Vijver DAMC, de Swart RL, Haagmans BL, et al. Intrathecal CD4+ and CD8+ T-cell responses to endogenously synthesized candidate disease-associated human autoantigens in multiple sclerosis patients. Eur J Immunol. 2016;46(2):347–53.

100. van Nierop GP, Mautner J, Mitterreiter JG, Hintzen RQ, Verjans GM. Intrathecal CD8+ T cells of multiple sclerosis patients recognize lytic Epstein-Barr virus proteins. Mult Scler J. 2015;22(3):279–91.

101. Murray PG, Young LS. Epstein–Barr virus infection: basis of malignancy and potential for therapy. Expert Rev Mol Med [serial online]. 2004 [cited 2018 Jan

6]. 2001;3(28):1–20. Available from: https://www.cambridge.org

102. Yadav S, Libotte F, Buono E, Valia S, Farina GA, Faggioni A, et al. EBV early lytic protein BFRF1 alters emerin distribution and post-translational modification. Virus Res [serial online]. 2017 [cited 2018 Jan 6];232(2):113–22. Available from: http://linkinghub.elsevier.com

103. Zur Hausen H, Schulte-Holthausen H, Klein G, Henle G, Henle W, Clifford P, et al. Epstein-Barr virus in Burkitt's lymphoma and nasopharyngeal carcinoma: EBV DNA in biopsies of Burkitt tumours and anaplastic carcinomas of the nasopharynx. Nature [serial online]. 1970 [cited 2018 Jan 6];228(1):1056–8. Available from: https://www.cabdirect.org

104. Chau CM, Zhang X-Y, McMahon SB, Lieberman PM. Regulation of Epstein-Barr Virus Latency Type by the Chromatin Boundary Factor CTCF. J Virol [serial online]. 2006 [cited 2018 Jan 6];80(12):5723–32. Available from: http://jvi.asm.org

105. Sivachandran N, Wang X, Frappier L. Functions of the Epstein-Barr Virus EBNA1 protein in viral reactivation and lytic infection. J Virol. 2012;86(11):6146–58.

106. Sugden B, Warren N. A promoter of Epstein-Barr virus that can function during latent infection can be transactivated by EBNA-1, a viral protein required for viral DNA replication during latent infection. J Virol [serial online]. 1989 [cited 2018 Jan 6];63(6):2644–9. Available from: http://www.pubmedcentral.nih.gov

107. Longnecker R, Miller CL, Miao XQ, Tomkinson B, Kieff E. The last seven transmembrane and carboxy-terminal cytoplasmic domains of Epstein-Barr virus latent membrane protein 2 (LMP2) are dispensable for lymphocyte infection and

growth transformation in vitro. J Virol [serial online]. 1993 [cited 2018 Jan 6];67(4):2006–13. Available from: http://www.pubmedcentral.nih.gov

108. Iwakiri D, Takada K. Role of EBERs in the Pathogenesis of EBV Infection: Research GFVW and GKBT-A in C, editor. Adv Cancer Res [serial online]. 2010 [cited 2018 Jan 6];107(1):119–36. Available from: http://www.sciencedirect.com

109. Sugimoto M, Tahara H, Ide T, Furuichi Y. Steps involved in immortalization and tumorigenesis in human B-lymphoblastoid cell lines transformed by Epstein-Barr virus. Cancer Res. 2004;64(10):3361–4.

110. Decker LL, Klaman LD, Thorley-Lawson DA. Detection of the latent form of Epstein-Barr virus DNA in the peripheral blood of healthy individuals. J Virol [serial online]. 1996 [cited 2018 Jan 6];70(5):3286–9. Available from: http://www.ncbi.nlm.nih.gov/pubmed

111. Rose C, Green M, Webber S, Day R, Watkins S, Reyes J, et al. Detection of Epstein-Barr virus genomes in peripheral blood B cells from solid-organ transplant recipients by fluorescence in situ hybridization. Clin Microbiol Infect. 2002;40(7):2533–44.

112. Ramayanti O, Juwana H, Verkuijlen SAMW, Adham M, Pegtel MD, Greijer AE, et al. Epstein-Barr virus mRNA profiles and viral DNA methylation status in nasopharyngeal brushings from nasopharyngeal carcinoma patients reflect tumor origin. Int J Cancer. 2017;140(1):149–62.

113. Liu X, Tang J, Wang M, Ma Q, Wang Y. Visual detection and evaluation of latent and lytic gene expression during Epstein-Barr virus infection using one-step reverse transcription loop-mediated isothermal amplification. Int J Mol Sci. 2013;14(12):23922–40.

114. Johnson KH, Webb C-H, Schmeling DO, Brundage RC, Balfour HH. Epstein–Barr virus dynamics in asymptomatic immunocompetent adults: an intensive 6-month study. Clin Transl Immunol [serial online]. 2016 [cited 2018 Jan 6];5(5):81. Available from: http://www.nature.com

115. Cocuzza CE, Piazza F, Musumeci R, Oggioni D, Andreoni S, Gardinetti M, et al. Quantitative detection of Epstein-Barr virus DNA in cerebrospinal fluid and blood samples of patients with relapsing-remitting multiple sclerosis. PLoS One. 2014;9(4):1–6.

116. Vo JH, Nei WL, Hu M, Phyo WM, Wang F, Fong KW, et al. Comparison of circulating tumour cells and circulating cell-free Epstein-Barr virus DNA in patients with nasopharyngeal carcinoma undergoing radiotherapy. Sci Rep [serial online]. 2016 [cited 2018 Jan 6];6(1):13. Available from: http://www.nature.com

117. Trypsteen W, Kiselinova M, Vandekerckhove L, De Spiegelaere W. Diagnostic utility of droplet digital PCR for HIV reservoir quantification. J Virus Erad [serial online]. 2016 [cited 2018 Jan 6];2(3):162–9. Available from: http://www.ncbi.nlm.nih.gov/pubmed

118. Kimura H, Miyake K, Yamauchi Y, Nishiyama K, Iwata S, Iwatsuki K, et al. Identification of Epstein-Barr virus (EBV)– infected lymphocyte subtypes by flow cytometric in situ hybridization in EBV-associated lymphoproliferative diseases. J Infect Dis. 2009;200(10):1078–87.

119. Just T, Burgwald H, Broe MK. Flow cytometric detection of EBV (EBER snRNA) using peptide nucleic acid probes. J Virol Methods [serial online]. 1998 [cited 2018 Jan 6];73(2):163–74. Available from: http://www.ncbi.nlm.nih.gov

120. Li R, Rezk A, Miyazaki Y, Hilgenberg E, Touil H, Shen P, et al.

Proinflammatory GM-CSF–producing B cells in multiple sclerosis and B cell depletion therapy. Sci Transl Med [serial online]. 2015 [cited 2018 Jan 6];7(310):166. Available from: http://stm.sciencemag.org

121. Haugen M, Frederiksen JL, Degn M. B cell follicle-like structures in multiple sclerosis-With focus on the role of B cell activating factor. J Neuroimmunol [serial online]. 2014 [cited 2018 Jan 6];273(1–2):1–7. Available from: http://dx.doi.org

122. Krumbholz M, Derfuss T, Hohlfeld R, Meinl E. B cells and antibodies in multiple sclerosis pathogenesis and therapy. Nat Rev Neurol [serial online]. 2012 [cited 2018 Jan 6];8(11):613–23. Available from: http://dx.doi.org

123. Sisay S, Lopez-Lozano L, Mickunas M, Quiroga-Fernández A, Palace J, Warnes G, et al. Untreated relapsing remitting multiple sclerosis patients show antibody production against latent Epstein Barr Virus (EBV) antigens mainly in the periphery and innate immune IL-8 responses preferentially in the CNS. J Neuroimmunol. 2017;306(2):40–5.

124. Fryer JF, Heath AB, Minor PD, Kessler H, Rawlinson W, Boivin G, et al. A collaborative study to establish the 1st WHO International Standard for human cytomegalovirus for nucleic acid amplification technology. Biologicals. 2016;44(4):242–51.

125. Waugh C, Cromer D, Grimm A, Chopra A, Mallal S, Davenport M, et al. A general method to eliminate laboratory induced recombinants during massive, parallel sequencing of cDNA library. Virol J [serial online]. 2015 [cited 2018 Jan 6];12(1):55. Available from: http://www.virologyj.com

126. Bio-Rad. Real-Time PCR Applications Guide [document on the Internet]. Bio-

Rad Applications Guide. 2006 [cited 2017 Oct 1]. p. 2–4. Available from: http://www.bio-rad.com/webroot/web/pdf/lsr/literature/Bulletin_5279.pdf

127. Heller M, Flemington E, Kieff E, Deininger P. Repeat arrays in cellular DNA related to the Epstein-Barr virus IR3 repeat. Mol Cell Biol. 1985;5(3):457–65.

128. Rennekamp AJ, Lieberman PM. Initiation of Epstein-Barr virus lytic replication requires transcription and the formation of a stable RNA-DNA hybrid molecule at OriLyt. J Virol [serial online]. 2011 [cited 2018 Jan 6];85(6):2837–50. Available from: http://jvi.asm.org

129. Buelow D, Sun Y, Tang L, Gu Z, Pounds S, Hayden R. Comparative Evaluation of Four Real-Time PCR Methods for the Quantitative Detection of Epstein-Barr Virus from Whole Blood Specimens. J Mol Diagn [serial online]. 2016 [cited 2018 Jan 6];18(4):527–34. Available from: http://www.sciencedirect.com

130. Dorner M, Zucol F, Berger C, Byland R, Melroe GT, Bernasconi M, et al. Distinct ex vivo susceptibility of B-cell subsets to Epstein-Barr virus infection according to differentiation status and tissue origin. J Virol [serial online]. 2008 [cited 2018 Jan 6];82(9):4400–12. Available from: http://jvi.asm.org

131. Kurth J, Spieker T, Wustrow J, Strickler JG, Hansmann M-L, Rajewsky K, et al. EBV-Infected B Cells in infectious mononucleosis. Immunity [serial online]. 2000 [cited 2018 Jan 6];13(4):485–95. Available from: http://dx.doi.org

132. Shiel WC. Multiple Sclerosis (MS) Symptoms, Treatment [document on the Internet]. OnHealth. 2016 [cited 2017 May 24]. Available from: http://www.onhealth.com/content/1/multiple_sclerosis_ms